ROR2 Regulates Cellular Plasticity in Pancreatic Neoplasia and Adenocarcinoma

Simone Benitz[1], Alec Steep[2], Malak M. Nasser[1], Jonathan Preall[3], Ujjwal Mukund Mahajan[4], Holly McQuithey[1], Ian Loveless[5], Erick T. Davis[1], Hui-Ju Wen[1], Daniel W. Long[1], Thomas Metzler[6], Samuel Zwernik[1], Michaela Louw[1], Donald Rempinski[1], Daniel J. Salas-Escabillas[1], Sydney M. Brender[1], Linghao Song[2], Ling Huang[1], Brian K. Theisen[7], Zhenyu Zhang[2], Nina G. Steele[1,8,9,10], Ivonne Regel[4], Filip Bednar[11] and Howard C. Crawford[1,9,10]

[1] *Department of Surgery, Henry Ford Health System, Detroit, Michigan, USA*

[2] *Center of Translational Data Science, University of Chicago, Chicago, Illinois, USA*

[3] *Cold Spring Harbor Laboratory Cancer Center, Cold Spring Harbor, New York, USA*

[4] *Department of Medicine II, University Hospital, LMU Munich, Munich, Germany*

[5] *Department of Public Health Sciences, Henry Ford Health System, Detroit, Michigan, USA*

[6] *Comparative Experimental Pathology (CEP), Institute of Pathology, School of Medicine and Health, Technical University of Munich, Munich, Germany*

[7] *Department of Pathology, Henry Ford Health, Detroit, Michigan, USA*

[8] *Department of Pathology, Wayne State University, Detroit, Michigan, USA*

[9] *Department of Pharmacology and Toxicology, Michigan State University, Lansing, Michigan, USA*

[10] *Department of Oncology, Wayne State University, Detroit, Michigan, USA*

[11] *Department of Surgery, University of Michigan, Ann Arbor, Michigan, USA*

Running Title: ROR2 in Pancreatic Cancer Cell Plasticity

Corresponding Author: Howard C. Crawford, PhD, Department of Surgery, Henry Ford Health System, Detroit, Michigan, USA

Email: hcrawfo1@hfhs.org

The authors declare no potential conflicts of interest.

Downloaded from http://aacrjournals.org/cancerdiscovery/article-pdf/doi/10.1158/2159-8290.CD-24-0137/3472265/cd-24-0137.pdf by Cold Spring Harbor Laboratory user on 15 July 2024

Abstract

Cellular plasticity is a hallmark of pancreatic ductal adenocarcinoma (PDAC) starting from the conversion of normal cells into precancerous lesions, to the progression of carcinoma subtypes associated with aggressiveness and therapeutic response. We discovered that normal acinar cell differentiation, maintained by the transcription factor Pdx1, suppresses a broad gastric cell identity that is maintained in metaplasia, neoplasia, and the classical subtype of PDAC in mouse and human. We have identified the receptor tyrosine kinase Ror2 as marker of a gastric metaplasia-like identity in pancreas neoplasms. Ablation of *Ror2* in a mouse model of pancreatic tumorigenesis promoted a switch to a gastric pit cell identity that largely persisted through progression to the classical subtype of PDAC. In both human and mouse pancreatic cancer, ROR2 activity continued to antagonize the gastric pit cell identity, strongly promoting an epithelial to mesenchymal transition, conferring resistance to KRAS inhibition, and vulnerability to AKT inhibition.

Significance

We discovered the receptor tyrosine kinase ROR2 as an important regulator of cellular identity in pancreatic precancerous lesions and pancreatic cancer. ROR2 drives an aggressive PDAC phenotype and confers resistance to KRAS inhibitors, suggesting that targeting ROR2 will enhance sensitivity to this new generation of targeted therapies.

Downloaded from http://aacrjournals.org/cancerdiscovery/article-pdf/doi/10.1158/2159-8290.CD-24-0137/3472265/cd-24-0137.pdf by Cold Spring Harbor Laboratory user on 15 July 2024

INTRODUCTION

Pancreatic ductal adenocarcinoma (PDAC) is a deadly disease with few curative options for the vast majority of patients, in part because early detection methods are lacking. PDAC is marked by extensive tumor cell heterogeneity comprised of “classical” and “basal-like” molecular subtypes that, instead of acting as stable cellular communities, exist on a spectrum, with plasticity between subtypes likely contributing to therapeutic resistance (1-3). Cellular plasticity is a hallmark of pancreatic cancer throughout progression, including transdifferentiation of normal cells into precancerous metaplastic and neoplastic lesions accompanied by the acquisition of distinct cellular identities. Whether cellular plasticity in precancerous disease is reflected in late-stage cancer progression has not been thoroughly considered, though some studies suggest a connection (4,5).

Both pancreatic duct and acinar cells can give rise to PDAC in mouse models (6-8). Acinar cells are more amenable to transformation in mice (8) and epigenetic analysis in patient samples suggests an acinar cell of origin (9). Inflammation or expression of oncogenic $Kras^{G12D}$ induces transdifferentiation of acinar cells to duct-like progenitor cells, a process called acinar-to-ductal metaplasia (ADM) (6,7,10). Metaplastic duct cells are characterized by an up-regulation of genes that define normal duct cells, such as *Krt19* and *Sox9,* and by loss of acinar differentiation markers, such as those encoding digestive enzymes (8,11,12).

The great majority of adult acinar cells are resistant to $Kras^{G12D}$-induced transformation, but in combination with the ablation of transcription factors that otherwise maintain acinar cell identity, such as *Hnf1a*, *Nr5a2*, *Mist1*, *Ptf1a* and *Pdx1*, transformation is significantly accelerated (13-17). Of these, genetic variants in *HNF1A*, *NR5A2* and *PDX1* are associated with susceptibility to PDAC development in patients (14,18). These findings support the hypothesis that maintenance of acinar cell identity is a powerful suppressor of pancreatic cancer initiation.

Downloaded from http://aacrjournals.org/cancerdiscovery/article-pdf/doi/10.1158/2159-8290.CD-24-0137/3472265/cd-24-0137.pdf by Cold Spring Harbor Laboratory user on 15 July 2024

In both injury and neoplasia models, metaplastic ducts show a high degree of cellular heterogeneity with subpopulations marked by senescent and proliferative characteristics and a variety of gastric cell identities including gastric chief-, pit-, tuft-, and enteroendocrine-like cells (19). In the stomach, chief cells secrete digestive enzymes and pit cells produce mucins that protect the epithelium from gastric juice (20); the functions of the chief and pit cell-like populations in pancreatic neoplasia are unclear. Notably, in experimental pancreatitis, a subset of metaplastic duct cells also assume a gastric SPEM (Spasmolytic Polypeptide-Expressing Metaplasia) identity (21). In the stomach, SPEM arises after glandular injury from corpus chief cells and SPEM cells characteristically co-express markers of gastric chief and mucous neck cells, such as Pepsinogen C (Pgc) and Mucin6 (Muc6), respectively (22).

While gastric cell identity is evident in pancreatic precancerous lesions, it has not been noted in carcinomas, which are instead marked by the classical and basal-like subtypes. The classical subtype exhibits higher expression of pancreatic lineage- and epithelial-defining transcription factors, whereas the basal-like subtype is characterized by an erosion of epithelial cell identity and acquisition of mesenchymal and basal cell features (23-27). Importantly, subtype identity of pancreatic cancer cells is associated with prognosis, with the basal-like subtype correlating to poorer overall survival (1).

The complex heterogeneity in both precancerous lesions and carcinoma has been of intense interest. Unfortunately, the study of the earliest molecular changes associated with the reprogramming of normal pancreatic acinar cells to neoplasia has been challenging using standard single-cell RNA-sequencing methods, largely due to the fragility of normal acinar cells during tissue disruption, together with high levels of digestive enzymes, especially nucleases. To overcome this, we performed single-nucleus ATAC-sequencing (snATAC-seq) of undigested, rapidly pulverized, frozen bulk mouse pancreas tissue to identify possible mechanisms of cellular reprogramming initiated by the inducible ablation of the acinar cell identity factor *Pdx1*, the expression of oncogenic $Kras^{G12D}$, or both together. Strikingly, chromatin accessibility of marker genes

Downloaded from http://aacrjournals.org/cancerdiscovery/article-pdf/doi/10.1158/2159-8290.CD-24-0137/3472265/cd-24-0137.pdf by Cold Spring Harbor Laboratory user on 15 July 2024

was sufficient to determine cell identity of multiple cell types within the tissues, including epithelial, fibroblast and immune cell populations. In transformation-sensitive *Pdx1*-null acinar cells, we identified increased accessibility and expression of several genes associated with a gastric SPEM signature, which was intensified in acinar cells also expressing *Kras*^{G12D}. Among these genes, we focused on *Ror2*, which encodes a receptor tyrosine kinase in the noncanonical *Wnt* signal transduction pathway. Genetic ablation of *Ror2* in a mouse model of pancreatic neoplasia shifted cell identity, giving rise to precancerous lesions dominated by mucinous gastric pit-like cells. In PDAC, *ROR2* expression strongly correlated with a basal-like/mesenchymal phenotype where it controls cell proliferation. Forcing *ROR2* expression in classical subtype PDAC cell lines was sufficient to induce a complete conversion to rapidly proliferating, poorly differentiated mesenchymal cells. The concomitant shift in signal transduction induced by ROR2 expression conferred resistance to a KRAS^{G12D} inhibitor while introducing a profound sensitivity to AKT inhibition.

RESULTS

Tracking Cell Identity Changes in Early Pancreatic Cancer Development Using snATAC-seq

To initiate pancreatic tumorigenesis, oncogenic Kras must overcome resistance to transformation posed by acinar cell identity (13-17,28). In order to study the earliest steps in this process, we compared pancreata with conditional adult acinar cell specific expression of Kras^{G12D} alone, to those also lacking Pdx1, a developmental transcription factor that we have shown previously to be important for maintaining acinar cell differentiation (17). We used *Ptf1aCre*^{ERT}-driven recombination to activate *Kras*^{G12D} expression and ablate *Pdx1* by treating 8- to 9-week-old mice with Tamoxifen, followed by tissue collection 2 and 10 weeks later to capture early progressive cell identity changes. Sole expression of *Cre*^{ERT} (*Ptf1a*^{ERT}) and loss of *Pdx1* (*Ptf1a*^{ERT}*;Pdx1*$^{f/f}$) did not cause any obvious morphological changes in the epithelial compartment, with the majority of cells being amylase-positive acinar cells (**Fig. 1A**, **1B**). Oncogenic Kras expression in *Ptf1aCre*^{ERT}*;Kras*$^{LSL\text{-}G12D}$ (*Ptf1a*^{ERT}*;K**) mice led to sporadic acinar-to-

Downloaded from http://aacrjournals.org/cancerdiscovery/article-pdf/doi/10.1158/2159-8290.CD-24-0137/3472265/cd-24-0137.pdf by Cold Spring Harbor Laboratory user on 15 July 2024

ductal metaplasia, characterized by loss of amylase, expression of the ductal marker Krt19, and a surrounding stromal reaction indicated by vimentin staining (**Fig. 1A**, **1B**). In contrast to the low metaplastic transformation efficiency of $Kras^{G12D}$ alone, the concomitant loss of Pdx1 significantly accelerated cellular reprogramming in *Ptf1aCre^{ERT};Kras$^{LSL\text{-}G12D}$;Pdx1$^{flox/flox}$* (*Ptf1a^{ERT};K*;Pdx1$^{f/f}$*) animals, as previously reported (17). Only 10 weeks after Tamoxifen, acinar cells had completely transdifferentiated into metaplastic duct-like cells, accompanied by a fibroinflammatory stromal reaction (**Fig. 1A**, **1B**).

To better define how *Kras^{G12D}* expression alone and in combination with *Pdx1* ablation impacts acinar cell identity, we established a novel protocol allowing high-quality snATAC-seq of snap-frozen, rapidly pulverized bulk pancreatic tissue (**Suppl. Fig. 1A**). Overall, this protocol allows for very rapid processing of samples, strongly preserving cellular identity. After extensive quality control and removal of low-quality nuclei (**Suppl. Fig. 1B**, **1C**), we performed downstream analysis with a total of 33,505 nuclei and compared chromatin accessibility states of *Ptf1a^{ERT}* and *Ptf1a^{ERT};Pdx1$^{f/f}$* control animals to mice with *Kras^{G12D}* expression, sacrificed 2 and 10 weeks post Tamoxifen.

Based on chromatin accessibility at the gene body and promoter, we calculated predicted gene expression activity scores by using the Signac pipeline (29) and used top predicted differentially accessible genes as well as previously established marker genes to assign cell cluster identity (**Suppl. Fig. 1D**, **1E**). We identified acinar, ductal and meta/neoplastic cells as well as fibroblasts, mesothelial, endothelial, immune and islet cells (**Fig. 1C**, **Suppl. Fig. 1E**). Surprisingly, although appearing morphologically normal, acinar cells of different mouse genotypes grouped into very distinct cell clusters, while other cell types remained unperturbed across genotypes at this resolution. Notably, acinar cells of *Ptf1a^{ERT}* control (Acinar, yellow cluster) and *Ptf1a^{ERT};K** (K* Acinar, brown cluster) mice showed slight differences, while acinar cells of *Pdx1* knockout mice (Pdx1$^{f/f}$ Acinar, orange cluster) exhibited an obvious switch of cell identity, independent of Kras status (**Fig. 1C**, **Suppl. Fig. 1E**). Acinar cell clusters were defined by predicted expression of digestive enzymes, such as *Cela1* and *Cpa1*. *Cela1*

Downloaded from http://aacrjournals.org/cancerdiscovery/article-pdf/doi/10.1158/2159-8290.CD-24-0137/3472265/cd-24-0137.pdf by Cold Spring Harbor Laboratory user on 15 July 2024

showed lower expression levels in acinar cells of *Ptf1a^{ERT};K** and *Ptf1a^{ERT};K*;Pdx1$^{f/f}$* animals, an indicator of distinct differentiation states (**Fig. 1D**). Consistent with the histology, expression of *Kras^{G12D}* led to time- and genotype-dependent meta/neoplastic duct cell formation (teal cluster), characterized by expression of metaplastic and ductal marker genes, such as *Onecut2* and *Hnf1b*, respectively (**Fig. 1C**, **1D**, **1E**). These data were consistent with the rampant metaplastic and neoplastic transformation in *Ptf1a^{ERT};K*;Pdx1$^{f/f}$* animals 10 weeks post Tamoxifen, with acinar cells being almost completely absent, replaced by an immense increase in meta/neoplastic duct cells (**Fig. 1C**, **1E**). These massive changes in the epithelial compartment were accompanied by a substantial increase of fibroblasts (light-green cluster), with little change in immune cell numbers (violet cluster) (**Fig. 1E**). Of note, the desmoplastic reaction in these mice made tissue digestion and isolation of high-quality nuclei more challenging, resulting in a lower overall number (**Fig.1C**).

Our snATAC-seq approach corroborated histological observations and changes in cell populations that occur during the early stages of tumorigenesis of the pancreas. Importantly, we uncovered that acinar cells from different mouse genotypes segregate into distinct clusters with an obvious shift in identity in metaplastic transformation-sensitive *Pdx1*-null acinar cells, revealing previously elusive details of early cellular reprogramming. We next sought to investigate gene accessibility changes among our identified acinar cell clusters in more detail.

Ablation of Pdx1 Initiates Gastric Transdifferentiation

To unmask cell identity differences across our acinar cell clusters, we subsetted acinar cells from the 2-week time point based on their genotype (**Fig. 2A**). To validate the identification of differentially regulated genes, we used an integrative approach combining our snATAC-seq with bulk RNA-seq data of isolated acinar cells from matching mouse genotypes and sex. Genes that showed the highest correlation across the two techniques are depicted in Figure 2B (**Fig. 2B**, **Suppl. Fig. 2A**). One gene confirming the validity of this approach was *Kdm6a*, which is located on the X chromosome and was both more accessible and more highly expressed in females

Downloaded from http://aacrjournals.org/cancerdiscovery/article-pdf/doi/10.1158/2159-8290.CD-24-0137/3472265/cd-24-0137.pdf by Cold Spring Harbor Laboratory user on 15 July 2024

(**Fig. 2B**). Acinar cells with Pdx1 loss exhibited an obvious decrease of accessibility and expression of acinar differentiation genes, such as *Cela1* or *Ptf1a* (17), but elevated levels of the AP-1 transcription factor *Junb*, which is associated with transcriptional reprogramming in ADM (30) (**Fig. 2B**, **Suppl. Fig. 2A**).

Among the top genes that showed the most significant enrichment in accessibility and expression in metaplastic transformation-sensitive *Pdx1*-null acinar cells was the receptor tyrosine kinase *Ror2* (Receptor Tyrosine Kinase Like Orphan Receptor 2) (**Fig. 2B**, **Suppl. Fig. 2A**). Ror2 regulates non-canonical Wnt signaling and defines cancer cell identity in a variety of tumor types (31-33). Besides *Ror2*, unsupervised clustering analysis of the RNA-seq data revealed that gastric lineage-specific genes, including *Cobalamin binding intrinsic factor* (*Cblif*), *Pepsinogen5* (*Pga5*), *Gastrokine3* (*Gkn3*) and *Aquaporin5* (*Aqp5*) (34,35) are up-regulated in *Pdx1*-knockout acinar cells, while acinar differentiation genes are down-regulated (**Fig. 2C, Suppl. Fig. 2B**). Considering that the acquisition of gastric signatures has recently been identified as a hallmark of pancreatic tumorigenesis (19,36), we asked if Ror2 itself is associated with gastric cell identity.

Analysis of published mouse scRNA-seq data derived from whole stomach tissue (19) indeed revealed *Ror2* expression in 3 distinct gastric cell populations (**Fig. 2D**). For gastric cell type annotation, we used a previously annotated mouse scRNA-seq dataset generated from the combined gastric corpus and antral regions (34) and found that the *Ror2*-expressing population 1 is associated with an endocrine, enterochomaffin-like cell identity, while populations 2 and 3 show an enrichment of gastric neck cell markers (**Fig. 2D**, **Suppl. Fig. 2C**). In accordance with our RNA-seq data from acinar cells, we detected some cells that co-express *Ror2* with *Cblif* and *Aqp5* in the stomach (**Fig. 2C**, **Fig. 2D**). IHC analysis of mouse stomach demonstrated Ror2 protein expression at the base, including Aqp5-positive deep antral neck cells in the antrum (**Suppl. Fig. 2D**). Of note, gene expression patterns of deep antral cells share characteristics of gastric metaplasia (SPEM), which forms in the corpus region upon gastric injury as part of a wound-healing program. SPEM cells arise from corpus chief cells, co-express chief and neck cell markers and resemble normal deep antral cells (22). The SPEM cell identity

Downloaded from http://aacrjournals.org/cancerdiscovery/article-pdf/doi/10.1158/2159-8290.CD-24-0137/3472265/cd-24-0137.pdf by Cold Spring Harbor Laboratory user on 15 July 2024

has been recently identified in pancreatitis-induced metaplasia (21), a putative precursor to neoplasia.

In addition to *Ror2*, we found that SPEM-associated genes, such as *Gkn3*, *Aqp5* (gastric neck cell markers) and *Pgc* (chief cell marker) were up-regulated in acinar cells with Pdx1 ablation, especially in combination with oncogenic Kras expression (**Fig. 2C**). Gene set enrichment analysis (GSEA) for previously published SPEM marker (21,37-39) confirm that the SPEM signature is significantly up-regulated in *Ptf1a^{ERT};K*;Pdx1$^{f/f}$* acinar cells (**Fig. 2E**). Thus, Pdx1 actively maintains acinar cell identity while it suppresses a gastric/SPEM identity and susceptibility to neoplastic transformation by Kras^{G12D}. Notably, we identified *Ror2* as a previously-unrecognized marker of the gastric cell identity-associated gene signature.

Ror2 Marks Gastric Neck Cell and SPEM Signatures in Pancreatic Neoplasia

Given that oncogenic Kras-induced meta/neoplastic cells in the pancreas acquire features reminiscent of gastric cell lineages (19,36), we examined if Ror2 expression was associated with this identity shift. By performing RNA-ISH and IHC, we found that Ror2 is indeed expressed in a portion of meta/neoplastic cells in *Ptf1a^{ERT};K** animals, comprising ~25% of Krt19-positive cells, especially in later time points (**Fig. 3A**). To explore whether *Ror2* expression levels define meta/neoplastic duct cell identity, we used pancreas scRNA-seq data from Schlesinger et al., which contained 3309 lineage-traced meta/neoplastic cells isolated from *Ptf1a^{ERT};K*;ROSA$^{LSL\text{-}TdTomato}$* mice (19) (**Fig. 3B**). In concordance with our IHC data, *Ror2* is expressed in subpopulations of tdTomato-positive meta/neoplastic cells (**Fig. 3B**). To determine the identity of Ror2-positive cells, we examined the expression of gastric cell type signatures from normal mouse gastric epithelia (34) as well as typical SPEM genes. We found that the Ror2^{High} cell population (**Fig. 3B**, circled) is indeed associated with higher expression of gastric neck cell and SPEM signatures. Consequently, we named this cluster neck/SPEM cell-like (**Fig. 3C**).

In accordance with Schlesinger et al. (19), we identified a pit cell-like population, confirmed by *Tff1* expression, a dividing population marked by expression of *Mki67*, and

Downloaded from http://aacrjournals.org/cancerdiscovery/article-pdf/doi/10.1158/2159-8290.CD-24-0137/3472265/cd-24-0137.pdf by Cold Spring Harbor Laboratory user on 15 July 2024

a senescent population with high expression of tumor suppressor genes, such as *Cdkn2a* (**Fig. 3C**, **Suppl. Fig. 3A**, **3B**, **3C**). Three clusters did not exhibit clear segregation of marker gene expression, which we designated as “hybrid”. While the “acinar-like” cluster retained expression of acinar genes, expression of ductal genes, such as *Dcdc2a*, was enriched in the “duct-like” cell cluster (**Fig. 3C**, **Suppl. Fig. 3D**, **3E**). Of note, we found the highest expression of *Ror2* in the neck/SPEM cell-like cluster, followed by dividing and acinar-like meta/neoplastic cell populations (**Fig. 3D**). Among the top 10 genes that showed the highest correlation to *Ror2* expression, we found the gastric neck and SPEM marker *Muc6* as well as the SPEM genes *Aqp5*, *Gkn3* or *Pgc* (**Fig. 3D**, **3E**), reminiscent of the gene signature found in *Pdx1*-null acinar cells (**Fig. 2C**). Validation studies using multiplex IF/ISH staining confirmed co-localization of *Ror2* with *Muc6* expression in ductal lesions of *Ptf1a^{ERT};K** mice, 20-weeks post Tamoxifen (**Fig. 3F**). Moreover, we detected that a proportion of Ror2-positive meta/neoplastic cells indeed co-expressed Ki-67, while co-localization with Cdkn2a or Tff1 was rare (**Fig. 3G, 3H**, **3I**).

Interestingly, Ror2-positive lesions showed lower abundance of *Krt19* expression, consistent with the SPEM population found in injury-induced ADM (21) (**Fig. 3F**, **Suppl. Fig. 3F**). In a model of chronic pancreatitis (21), a substantial proportion of “Mucin/Ductal” cells also expressed *Ror2*, again showing correlation with neck cell and SPEM marker gene expression, such as *Muc6* or *Aqp5* (**Suppl. Fig. 3G**, **3H**, **3I**, **3J**). In summary, our data suggested that Ror2-positive meta/neoplastic cells are of a proliferative neck/SPEM cell identity, distinct from cells with senescent and pit-cell like features. Since the relevance of these cellular identities on pancreatic cancer development is unknown, we next sought to determine if ablation of the neck/SPEM marker Ror2 impacts carcinogenesis in mice.

Ror2 Ablation Shifts Gastric Metaplasia Towards a Pit Cell Identity

To assess the functional relevance of Ror2 in early metaplasia and neoplasia, we generated *Ptf1a^{ERT};K** mice with a conditional knockout allele of *Ror2* and a *ROSA$^{LSL\text{-}YFP}$* reporter. *Ptf1aCre^{ERT}*-mediated recombination led to the deletion of Exon3/4 of the

Downloaded from http://aacrjournals.org/cancerdiscovery/article-pdf/doi/10.1158/2159-8290.CD-24-0137/3472265/cd-24-0137.pdf by Cold Spring Harbor Laboratory user on 15 July 2024

Ror2 gene in the majority of acinar cells (**Suppl. Fig. 4A**). IHC for the YFP reporter expression suggested a recombination efficiency of ~90%. We noted that some lesions retained Ror2 expression, suggesting either less efficient recombination of this locus or possible selection for cells that escaped recombination (**Suppl. Fig. 4B**). While we observed slight differences in tissue remodeling, quantified as loss of acinar cells and formation of meta/neoplastic duct-like structures between *Ptf1a^{ERT};K** and *Ptf1a^{ERT};K*,Ror2$^{f/f}$* animals at 10 weeks post Tamoxifen (**Suppl. Fig. 4C)**, *Ptf1a^{ERT};K*,Ror2$^{f/f}$* animals presented with significantly more transformation at 20 and 40 weeks post Tamoxifen (**Fig. 4A**). Notably, 40 weeks post Tamoxifen, 3 *Ptf1a^{ERT};K*,Ror2$^{f/f}$* mice developed regions of carcinoma, a rapidity of progression not observed in our control cohort. They also showed a more pronounced stromal reaction with significantly elevated collagen deposition as represented by Picrosirius Red stain, which was also observed when *Ror2* was ablated in a mammary cancer model (40) (**Suppl. Fig. 4D**). When comparing lesion identity in mice that presented with neoplasia, we found that *Ptf1a^{ERT};K*,Ror2$^{f/f}$* animals exhibit an increase in the number of mucinous meta/neoplastic lesions, the first indication of a possible shift in epithelial cell identity (**Fig. 4A**).

Based on our previous observation that Ror2 was mainly expressed in proliferative neck/SPEM subpopulations of meta/neoplastic cells, but negatively associated with senescent (Cdkn2a-positive) and pit-like (Tff1-positive) cells, we analyzed *Ror2* knockout mice for a possible shift in cellular identity. Characterization of Krt19-positive ductal structures at 20 weeks post Tamoxifen revealed that lesions in *Ror2* knockout mice were less proliferative and had a significantly higher number of Cdkn2a-positive senescent cells, with the senescent phenotype having abated by 40 weeks (**Fig. 4B**, **4C**). The high prevalence of mucinous lesions at 40 weeks led us to stain for Muc6, a SPEM marker, as well as Tff1 and Muc5ac, both markers for gastric pit cell identity. We observed a slight reduction of *Muc6*-expressing Krt19-positive cells (**Fig. 4D**), accompanied by a higher proportion of ductal cells expressing Muc5ac and Tff1 when *Ror2* was ablated (**Fig. 4E**, **4F**). This shift of cell identity also was evident in immunoblot

Downloaded from http://aacrjournals.org/cancerdiscovery/article-pdf/doi/10.1158/2159-8290.CD-24-0137/3472265/cd-24-0137.pdf by Cold Spring Harbor Laboratory user on 15 July 2024

analyses from bulk pancreatic tissue lysates confirming increased Tff1 levels in *Ror2-null*, *Kras*^{G12D}-expressing mice (**Fig. 4G**).

Altogether, these data show that ablation of *Ror2* promotes tissue transformation and fibrosis. *Ror2* ablation also shifted cellular identity of precancerous lesions, with an increased number exhibiting a mucinous Tff1-positive gastric pit cell-like identity and an overall higher likelihood of progression to PDAC. These two concurrent phenotypes suggest a possible connection between the pit-like phenotype and progression to carcinoma, a possibility bolstered by Tff1 also being a well-established marker for the classical PDAC molecular subtype (24,26).

Pit Cell Identity Marks the Classical Subtype of PDAC whereas Ror2 Expression Is Associated with the Basal-like Subtype

To assess if Ror2 and gastric gene signatures define subtype identity in PDAC, we turned to the well-established KPC (*Ptf1aCre;Kras*$^{LSL-G12D}$*;Trp53*^{R172H}) mouse model, which recapitulates human PDAC subtype heterogeneity, including the epithelial, classical and the more mesenchymal, basal-like subtypes (41). Dual IHC for Ror2 (brown) and Tff1 (teal) revealed that expression is very heterogeneous in neoplastic and carcinoma areas in KPC mice and confirmed that Ror2 and Tff1 define distinct, non-overlapping subpopulations (**Fig. 5A**). Accordingly, analysis of previously published RNA-seq data generated from mouse pancreatic cancer cell lines (42) also showed a significant negative correlation between the two genes. Moreover, while *Ror2*^{Low}*/Tff1*^{High} cells are characterized by a differentiated epithelial cell identity (clusters C2a-C2c), *Ror2*^{High}*/Tff1*^{Low} expressors are associated with a more mesenchymal cell differentiation state (C1) (**Fig. 5B**).

Using Pearson correlation analysis, we further uncovered that *Ror2* does not only negatively correlate to *Tff1*, but to a myriad of genes that define meta/neoplastic pit-like cells. Importantly, the great majority of most enriched pit cell-like marker genes (n=50) show a strong association with the classical subtype, including 9 genes (highlighted in red) that are part of a recently defined 30 gene human classical PDAC signature (27)

Downloaded from http://aacrjournals.org/cancerdiscovery/article-pdf/doi/10.1158/2159-8290.CD-24-0137/3472265/cd-24-0137.pdf by Cold Spring Harbor Laboratory user on 15 July 2024

(**Fig. 5C**). To validate these findings in human PDAC tissue, we surveyed publicly available scRNA-seq data from 174 human PDAC samples, to our knowledge, the largest aggregated collection of PDAC patient tissues (2,43-51). Ductal cells (*KRT18* and *KRT19* enriched, negative for acinar and other cell lineage markers) were subsetted from total cells and re-clustered in Seurat. GSEA within the ductal population revealed a tight overlap between the pit cell-like and the classical PDAC gene signature (**Fig. 5D**, **Suppl. Fig. 5A**). These data suggest that cell fate traits of meta/neoplastic pit-like cells are maintained in classical PDAC in mouse models and importantly, in patient tumors.

To identify cellular identity features that show high correlation to *Ror2*, we re-visited the RNA-seq data of mouse pancreatic cancer cell lines (42) given its large number of samples that represent classical or basal-like PDAC subtype identity. Strikingly, genes that show highest correlation to *Ror2* expression exhibit markedly elevated expression in the mesenchymal cell lines (C1) associated with the basal-like subtype, as defined by gene signatures from Moffitt et al. (23) (**Fig. 5E**). To elucidate the biological function of genes that positively and negatively correlated with *Ror2*, we conducted GO pathway analysis. *Ror2* positively-correlated genes were associated with cancer cell aggressiveness and EMT, whereas negatively-correlated genes were regulators of apoptosis or epithelial differentiation (**Suppl. Fig. 5B**). Interestingly, the most significantly enriched GO term for positively-correlated genes “multicellular organism development” contained a myriad of well-known EMT-inducing transcription factors, such as Prrx1, Snai1, Twist or Zeb family members. Correlation plots present significant positive correlation of *Ror2* with *Snai1*, *Twist1*, *Zeb1* or *Vimentin (Vim)* expression, while expression of epithelial genes *E-Cadherin (Cdh1)* and *Krt19* is negatively correlated with *Ror2* (**Fig. 5F**). Interestingly, *Ror2*-positive pancreatic cancer cells were associated with lower *Krt19* expression, a finding that we observed previously in Ror2-positive precancerous lesions.

ROR2 Induces EMT and Stemness in Human Pancreatic Cancer Cells

Downloaded from http://aacrjournals.org/cancerdiscovery/article-pdf/doi/10.1158/2159-8290.CD-24-0137/3472265/cd-24-0137.pdf by Cold Spring Harbor Laboratory user on 15 July 2024

Based on our finding that Ror2 correlated to the basal-like/mesenchymal PDAC subtype in mice, we asked if ROR2 showed a similar association in human PDAC. For this, we examined ROR2 expression in resected tumors, patient-derived organoids and cancer cell lines. Within ROR2-expressing tumor samples, we observed significant heterogeneity, with highest expression correlating to moderate to poorly differentiated carcinoma (**Fig. 6A**). Given that ROR2 is highly expressed in fibroblasts, which can confound analysis of bulk RNA-seq data from whole tumor tissue, we analyzed data from human micro-dissected PDAC epithelium (52) and found that *ROR2* expression correlates with the expression of EMT genes, such as *ZEB1* and *Vimentin*, whereas *E-Cadherin* and *EPCAM* inversely correlate (**Fig. 6B**). Of note, basal-like tumor samples are highly underrepresented in human PDAC, likely due to these aggressive tumors not usually qualifying for resection and downstream analysis. Accordingly, when we analyzed human organoid (**Suppl. Fig. 6A)** and pancreatic cancer cell lines, including primary patient lines, we found that the majority exhibited more epithelial characteristics and were negative for *ROR2* expression. However, all lines that did express ROR2 also showed mesenchymal features, such as Vimentin and ZEB1 expression, and extremely low levels of the E-Cadherin (**Fig. 6C**, **6D**). We conclude that ROR2 is strongly associated with a mesenchymal differentiation in human PDAC.

Next, we assessed if expression of *ROR2* in the epithelial cell lines HPAF-II and the primary patient cell line UM32 is sufficient to cause cellular reprogramming and a switch of cell identity. Notably, overexpression of ROR2 clearly induced EMT, characterized by loss of the epithelial and gain of the spindle-shaped, mesenchymal morphology (**Fig. 6E**). Immunofluorescence and immunoblot analyses demonstrated concomitant expression of the EMT markers ZEB1 and Vimentin, while E-Cadherin was completely lost (**Fig. 6E**, **6F**). Consequently, we compared RNA-seq data of HPAF-II and UM32 control and *ROR2*-overexpressing cells to the EMT signature established by Groger et al. (53). *ROR2*-overexpressing HPAF-II and UM32 cells displayed a significantly enriched EMT score compared to control cells (**Fig. 6G**). In addition, expression of previously identified classical PDAC subtype and pit cell marker genes were completely abrogated upon *ROR2* expression, overall indicating that ROR2 erodes pancreatic

Downloaded from http://aacrjournals.org/cancerdiscovery/article-pdf/doi/10.1158/2159-8290.CD-24-0137/3472265/cd-24-0137.pdf by Cold Spring Harbor Laboratory user on 15 July 2024

cancer cell identity and promotes acquisition of a mesenchymal phenotype (**Suppl. Fig. 6B**).

Previous studies revealed that activation of EMT programs induce stem cell features, with ZEB1 being a key factor for stemness in various cancer entities (4,54,55). Our RNA-seq data unveiled that the gastric stem cell genes *LGR5* or *CXCR4* are greatly upregulated upon expression of *ROR2* in HPAF-II and UM32 cells (**Suppl. Fig. 6C**). To test if this stem cell-like signature predicts function, we examined the ability of *ROR2*-expressing cells to form tumor spheres in low adhesion plates. Indeed, *ROR2*-expressing cells formed a significantly greater number and larger tumor spheres *in vitro* than control cells (**Fig. 6H**). Overall, our data identify ROR2 as a driver of human PDAC progression, inducing EMT and stemness.

ROR2 Confers a RAS-independent, AKT-dependent Proliferative Phenotype

Next, we studied the effects of ROR2 loss in the *ROR2*-expressing, mesenchymal PANC1 and UM5 cell lines. CRISPR/Cas9-mediated knockout using two different guide RNAs (ROR2 KO #1, ROR2 KO #2) had no consistent effect on EMT marker gene expression (**Suppl. Fig. 7A**), demonstrating that ROR2 signaling is not necessary for maintaining EMT once initiated. However, ablation of *ROR2* in PANC1 and UM5 led to a significant decrease in cell proliferation (**Fig. 7A**), an effect that was particularly dramatic in the patient-derived primary cell line UM5, so much so that recovery of RNA/protein or execution of functional assays were extremely challenging (**Suppl. Fig. 7B**). To study immediate ROR2 target genes, we performed siRNA-mediated acute knockdown of *ROR2* and performed RNA-seq. Top enriched GSEA gene sets in control versus *ROR2* knockdown cells were associated with fundamental regulators of proliferation, such as cell cycle-regulating E2F targets and G2/M transition genes (**Suppl. Fig. 7C**), an effect that has been observed in other tumor types (56,57). In contrast, ectopic overexpression of *ROR2* in the ROR2-negative cell lines HPAF-II and UM32 induced an extensive increase of cell proliferation (**Fig. 7B**), correlating with an up-regulation of E2F and G2/M target genes (**Suppl. Fig. 7D**).

Downloaded from http://aacrjournals.org/cancerdiscovery/article-pdf/doi/10.1158/2159-8290.CD-24-0137/3472265/cd-24-0137.pdf by Cold Spring Harbor Laboratory user on 15 July 2024

We next used exploratory phospho-Arrays to identify downstream signaling of ROR2 and confirmed these findings by immunoblot analysis. While *ROR2* knockout cells, especially UM5, showed a reduction in phospho-AKT levels, overexpression of *ROR2* led to a marked increase, accompanied by a virtual ablation of activated phospho-ERK (**Fig. 7C**, **7D**), a surprising effect considering both cell lines harbor mutant $KRAS^{G12D}$. To test if this profound shift away from ERK and towards AKT signaling would alter response to pharmacological inhibitors, we tested HPAF-II and UM32 *ROR2*-overexpressors' response to the $KRAS^{G12D}$ inhibitor MRTX1133 (**Fig. 7E**) and the AKT inhibitor MK-2206 (**Fig. 7F)**. Indeed, we found that *ROR2* expressing cells were more resistant to $KRAS^{G12D}$ inhibition compared to controls, but newly vulnerable to AKT inhibition.

DISCUSSION

Pancreatic cancer is an almost universally fatal disease marked by immense tumor cell heterogeneity that contributes to resistance to therapy (1). This tumor cell heterogeneity, in turn, is driven by the profound plasticity of the exocrine pancreas (58), a quality evident in acinar cell transdifferentiation to metaplastic duct-like cells in chronic pancreatitis, and in their susceptibility to form precancerous lesions induced by the expression of oncogenic Kras (19,21). In this study, we have applied single-nucleus ATAC-seq to capture early reprogramming of acinar cells induced by the expression of $Kras^{G12D}$, as well as in acinar cells with a compromised identity due to *Pdx1* ablation. We discovered that ablation of *Pdx1* alone initiates reprogramming towards a gastric cell identity, an effect also seen upon ablation of *Ptf1a*, another transcription factor critical for the maintenance of acinar cell identity (59). Gastric cell gene expression was intensified by the expression of $Kras^{G12D}$. Among the upregulated genes we identified was the non-canonical Wnt receptor Ror2, which we found is expressed in the deep antral cells of the stomach, together with many markers of gastric metaplasia (SPEM) (22).

Downloaded from http://aacrjournals.org/cancerdiscovery/article-pdf/doi/10.1158/2159-8290.CD-24-0137/3472265/cd-24-0137.pdf by Cold Spring Harbor Laboratory user on 15 July 2024

In progressive neoplasia in the mouse, we found that Ror2 remains associated with and promotes a proliferative neck cell/SPEM-like identity while its ablation resulted in more extensive neoplastic transformation. This is consistent with SPEM playing a wound healing function in neoplasia as it does in normal stomach and pancreas, possibly suppressing the progressive loss of normal tissue (60). Early neoplastic lesions lacking Ror2 were highly senescent while in late neoplasia the tissue became dominated by a gastric pit cell-like cell identity, suggesting that Ror2 is actively involved in maintaining cell identity. Interestingly, a subset (3/11) of *Ptf1a^{ERT};K*,Ror2$^{f/f}$* mice developed carcinoma at a very early 40-week time point, a progression speed not observed in control *Ptf1a^{ERT};K** animals either in this study or historically. The observation that the classical subtype of PDAC maintains a mostly pit cell-like identity signature leads us to hypothesize that the pit cell-like neoplastic cells are the immediate precursors to carcinoma. If this is the case, either their sheer numbers or their having selectively bypassed senescence and low proliferation earlier in progression would make PDAC more likely to form.

In PDAC, ROR2 expression is associated with an aggressive basal-like molecular subtype and a mesenchymal phenotype. Its ectopic expression in human PDAC cell lines with a classical subtype identity was sufficient to promote extensive reprogramming towards a mesenchymal, and highly proliferative phenotype, a function observed in other tumor types (31,32). Though it is possible that the Ror2-expressing neck/SPEM neoplasia is a precursor to basal PDAC, other than ROR2, we did not observe substantial expression of other SPEM markers in this subtype. It is perhaps more likely that ROR2 actively drives mesenchymal differentiation in a manner that reflects its role in fibroblasts, where it is consistently expressed in normal, neoplastic and cancerous pancreas.

Overall, our data point to a complex function of ROR2, resisting progression in precancerous stages and promoting progression in PDAC. Linking these two functions is ROR2's regulation of cellular plasticity. Cellular plasticity is increasingly recognized as a mechanism of therapeutic resistance in cancer (27,61). ROR2 has been shown to

Downloaded from http://aacrjournals.org/cancerdiscovery/article-pdf/doi/10.1158/2159-8290.CD-24-0137/3472265/cd-24-0137.pdf by Cold Spring Harbor Laboratory user on 15 July 2024

induce EMT in several tumor types (31-33,62), though its relationship to ERK (63-65) and AKT signaling pathways (65-67) appears to be highly context-dependent. We found that *ROR2* expression in two $KRAS^{G12D}$-mutated PDAC cell lines has a dramatic effect on the classic effector pathways downstream of KRAS, virtually eliminating ERK activity and drastically upregulating AKT activity. ROR2's hyperactivation of AKT was consistent with observations in several tumor types (66,67). This remarkable shift away from a dependency on ERK signaling presaged resistance to KRAS inhibition, while the hyperactivation of AKT created an increased vulnerability to AKT inhibition by MK-2206. To further explore its role in resistance to KRAS inhibition, we examined ROR2 expression in cell lines that have been selected for resistance to MRTX1133 *in vitro* and *in vivo* and found its expression inconsistent, suggesting that *ROR2* upregulation is not a common mechanism of acquired resistance. However, our data suggest that its expression within a subset of aggressive, basal-like PDACs is likely to be predictive of therapeutic efficacy of KRAS and AKT inhibitors.

In addition to targeting its downstream effectors, the recent advent of inhibitory small molecules and monoclonal antibodies (68,69) will also allow for direct targeting of ROR2 itself in the future. Another approach to targeting ROR2 activity is indirectly, by targeting its ligands. We consistently observed expression of the ROR2 ligand WNT5A in PDAC epithelia and stroma (data now shown) in accordance with other studies demonstrating its prevalent expression in primary tumors where it promotes EMT (70), as well as in subsets of circulating tumor cells from PDAC patients (71). However, treatment of our ROR2-expressing human PDAC cell lines with the Porcupine O-acyltransferase (PORCN) inhibitor LGK-974, an agent that inhibits post-translational modification and secretion of WNT ligands, did not reduce cell proliferation as we observed in our ROR2 knockout cells. This suggests that ROR2 may have WNT ligand-independent activities or that inhibition of both canonical and noncanonical WNTs together has more complicated effects than targeting the noncanonical arm alone.

In summary, we found that erosion of pancreatic acinar cell identity induced by *Pdx1* ablation was sufficient to confer a gastric identity gene signature that was maintained up

Downloaded from http://aacrjournals.org/cancerdiscovery/article-pdf/doi/10.1158/2159-8290.CD-24-0137/3472265/cd-24-0137.pdf by Cold Spring Harbor Laboratory user on 15 July 2024

to and including progression to the classical subtype of PDAC. Among the neck cell/SPEM subpopulation of metaplastic epithelium, we identified Ror2 to be a powerful regulator of cellular identity throughout progression. In early-stage disease, Ror2 suppresses neoplastic transformation and progression to PDAC. In carcinoma, ROR2 promotes progression to an aggressive basal-like subtype where it modulates therapeutic responses to KRAS and AKT inhibition.

METHODS

Cell Culture

The human pancreatic cancer cell lines PANC1 (RRID:CVCL_0480) and HPAF-II (RRID:CVCL_0313) were purchased from ATCC, UM5 and UM32 were kindly provided by Dr. Costas Lyssiotis (University of Michigan). Identity of cell lines was confirmed by STR analysis (University of Arizona). PANC1 were cultivated in Dulbecco's Modified Eagle Medium (DMEM) (10-013-CV, Corning), supplemented with 10% fetal bovine serum (FBS) (F2242, Thermo Fisher Scientific) and 0.5% Gentamicin (15-710-072, Fisher Scientific). HPAF-II cells were cultured in Minimum Essential Medium (MEM, 11-095-080, Fisher Scientific) containing 1% sodium pyruvate (11360070, Thermo Fisher Scientific), 1% non-essential amino acids (11140050, Thermo Fisher Scientific), 10% FBS and 0.5% Gentamicin. UM5 and UM32 were cultivated in RPMI 1640 (10-040-CV, Corning) with 10% FBS and 0.5% Gentamicin. 293FT cells were grown in DMEM supplemented with 1% sodium pyruvate, 1% non-essential amino acids, 10% FBS and 1% Penicillin/Streptomycin. Generally, cells were passaged at a confluency of ~80% by using Trypsin/EDTA (25200114, Thermo Fisher Scientific). All cell lines were regularly tested for mycoplasma using the MycoStrip-Mycoplasma Detection Kit (Rep-mys-50, Invivogen) and maintained at 37°C in a humidified chamber with saturated atmosphere containing 5% CO_2.

Organoid Culture

Organoid cultures 163, 265, 281 and 286 were previously established from PDX tumors (72). Organoids were maintained in Cultrex^{TM} UltiMatrix Reduced Growth Factor

Downloaded from http://aacrjournals.org/cancerdiscovery/article-pdf/doi/10.1158/2159-8290.CD-24-0137/3472265/cd-24-0137.pdf by Cold Spring Harbor Laboratory user on 15 July 2024

Basement Membrane Extract (BME001-10, R&D Systems) and incubated in Advanced DMEM/F12 (12-634-010, Thermo Fisher Scientific) culture medium, supplemented with human recombinant fibroblast growth factor-basic (FGF2) (100-18C, Peprotech), B27 (17504044, Thermo Fisher Scientific) and other factors (73). Culture medium was replaced every 2-3 days, and organoids were passaged every 12-14 days. For passaging, organoids were digested in 1 mg/ml collagenase-dispase solution (LS004106, Cedarlane) for 1.5 hours followed by 15 minutes TrypLE™ (12604021, Thermo Fisher Scientific) treatment. Dissociated organoid cells were washed, resuspended in Cultrex and seeded at a density of 20,000 cells per well of a 24 well-plate. After solidification, 1 mL of culture medium was added to each well.

Gene Editing / Overexpression Experiments

ROR2 knockout in PANC1 and UM5 cells was induced by using the eSpCas9-LentiCRISPRv2 vector system (74) containing the following guide RNA sequences: ROR2 guide RNA (gRNA) 1 (AGCCGCGGCGGATCATCATC), ROR2 gRNA 2 (ATGAAGACCATTACCGCCAC) or scrambled control gRNA (ACGGAGGCTAAGCGTCGCAA). For the generation of lentiviruses, 293FT cells were transfected with the target vector and the packaging plasmids pLP1, pLP2 and pLP/VSVG (Thermo Fisher Scientific) by using Lipofectamine 2000 (11668019, Thermo Fisher Scientific). Lentiviral particles were collected 72 hours after transfection and concentrated by using Lenti-X Concentrator (631231, Takara). After transduction, PANC1 and UM5 cells were constantly kept in cell culture medium containing 5 µg/ml and 2.5 µg/ml Puromycin (P8833, Millipore Sigma), respectively. ROR2 knockout was confirmed by Western Blot.

For overexpression of ROR2, pLV[Exp]-EGFP:T2A:Puro-EF1A>hROR2 (VB900004-2980bun,_VectorBuilder) or control vector pLV[Exp]-EGFP/Puro-EF1A>ORF_stuffer, (VB900021-9574dpn, VectorBuilder) were packaged into lentiviral particles, concentrated supernatant was added to HPAF-II and UM32 cells and cells were selected with Puromycin.

siRNA Transfection

Downloaded from http://aacrjournals.org/cancerdiscovery/article-pdf/doi/10.1158/2159-8290.CD-24-0137/3472265/cd-24-0137.pdf by Cold Spring Harbor Laboratory user on 15 July 2024

One day before siRNA transfection, cells were seeded in antibiotics-free cell culture medium. Cells were transfected with either 10 nM Silencer™ Select Negative Control #1 (4390843, Thermo Fisher Scientific) or siROR2 #1 (s9760, Thermo Fisher Scientific) resuspended in Opti-MEM I Reduced Serum Medium (31985062, Thermo Fisher Scientific) containing Lipofectamine2000. After six hours of incubation, cells were washed with PBS and cultivated in normal cell culture medium. Cells were harvested three and four days after transfection for RNA and protein isolation, respectively. Knockdown efficiency was ~70%.

Proliferation Assay

To estimate cell proliferation, 2,000 cells were seeded on a well of a 96-well plate and brightfield images were taken every two hours by using the BioTek BioSpa 8 Automated Incubator and Citation 5 reader (Agilent). BioTek Gen5 imaging software (Agilent) was used to determine cell confluency, which is generally represented as the mean of four wells.

Sphere Formation Assay

Spheroid formation was studied according to the clonal assay principle. For each experiment, single cells were seeded in wells of three, U-bottom shaped 96-well ultra-low attachment plates (CLS7007-24EA, Millipore Sigma). Cells were cultivated in serum-free RPMI 1640 medium containing B-27 supplement, 10 ng/ml FGF2, 20 ng/ml human recombinant epidermal growth factor (EGF) (AF-100-15, Peprotech), 10 mM HEPES (15-630-106, Thermo Fisher Scientific) and 0.5% Gentamicin. Spheroid cultures were kept for 14 days, number of spheres in relation to total number of seeded wells was assessed and sphere forming efficiency was calculated. Only spheres with a diameter > 75 µm were considered. Brightfield images were taken with the THUNDER Microscope Imager (Leica).

Drug Response Assay

For drug response assays, 4,000 cells/well were seeded in 100µl of appropriate media in a 96-well plate. After overnight incubation, cells received treatment with increasing

Downloaded from http://aacrjournals.org/cancerdiscovery/article-pdf/doi/10.1158/2159-8290.CD-24-0137/3472265/cd-24-0137.pdf by Cold Spring Harbor Laboratory user on 15 July 2024

concentrations of the $Kras^{G12D}$ inhibitor MRTX1133 (E1051, Selleckchem) and AKT inhibitor MK-2206 (S1078, Selleckchem). All vehicles were treated with 1% DMSO. Cell viability was assessed by using CellTiter-Glo 2.0 reagent (G9242, Promega). After 48-72 hours, 100 µl CellTiter-Glo 2.0 reagent was added to each well, followed by incubation of the plate on a shaker for 2 minutes using 120 rpm and 10 minutes incubation at room temperature. Luminescence was measured by using the SpectraMax iD3 (Molecular Devices). The average of each duplicate was calculated and normalized to the vehicle control. IC_{50} values were calculated using GraphPad Prism version 9.

Mouse Lines

The strains *Ptf1aCre*^{ERT}, *Pdx1*$^{f/f}$, *Kras*$^{LSL\text{-}G12D}$ and *R26R*$^{LSL\text{-}YFP}$ were previously described (17). *Ror2*$^{f/f}$ animals were purchased from the Jackson Laboratory (strain #018354) (75) and bred into *Ptf1aCre*$^{ERT/+}$;*Kras*$^{LSL\text{-}G12D}$ animals. To induce *Ptf1aCre*^{ERT}-dependent recombination, animals were treated with Tamoxifen (T5648, Sigma). Tamoxifen was dissolved in corn oil and administered by oral gavage, 5 mg daily for a total of five days. All animal procedures were approved by the University of Michigan and Henry Ford Health System Institutional Care and Use of Animal Committees.

Acinar Cell Isolation

Acinar cells were isolated from pancreas tissue as previously described (17). In brief, pancreas tissue was washed three times in Hank's Balanced Salt Solution (HBSS) (SH3026801, Thermo Fisher Scientific), minced and digested in HBSS containing 0.5 mg/ml Collagenase P (Roche, 11249002001) for 15 minutes at 37°C. Digestion reaction was stopped by washing the tissue three times in HBSS with 5% FBS. Acinar cells were isolated by straining the tissue through 500 µm and 100 µm filter meshes and centrifugating the cells through a gradient of 30% FBS in HBSS. Acinar cells designated for RNA-sequencing experiments were washed in PBS, resuspended in RLT buffer and RNA was immediately isolated.

PCR Genotyping of $Ror2^{NULL}$ Allele

Downloaded from http://aacrjournals.org/cancerdiscovery/article-pdf/doi/10.1158/2159-8290.CD-24-0137/3472265/cd-24-0137.pdf by Cold Spring Harbor Laboratory user on 15 July 2024

PCR-based genotyping of the *Ror2*^{NULL} allele was performed according to Ho et al. (75). In brief, acinar cells of *Ptf1a*^{ERT}*;K** and *Ptf1a*^{ERT}*;K*;Ror2*$^{f/f}$ mice were isolated one week after Tamoxifen administration and genomic DNA was isolated using the DNeasy® Blood and Tissue Kit (69504, Qiagen). PCR was performed using the Go Taq™ Master Mix (PRM7123, Promega).

Protein Extraction and Immunoblotting

For Western Blot analysis, cells were seeded at defined densities and lysed in RIPA buffer (10 mM Tris-HCl (pH 7.4), 150 mM NaCl, 0.1% SDS, 1% Na-deoxycholate and 1% Triton X-100) supplemented with protease (A32965, Thermo Fisher Scientific) and phosphatase inhibitors (4906837001, Millipore Sigma). Cell extracts were sonicated for 10 seconds and residual debris was pelleted by centrifugation (10 min, 18 400 g, 4°C). For protein extraction from pancreata, ~ 30 mg tissue was added to tissue lysis buffer (10 mM Tris-HCl (pH 7.4), 150 mM NaCl, 1 mM EDTA, 1% NP-40, 0.1% SDS, 0.5% Na-deoxycholate supplemented with protease and phosphatase inhibitors). Tissue was homogenized by using the Qiagen tissue lyser (3 min, 50 oscillations/s). Samples were sonicated and supernatant was extracted after centrifugation (20 min, 18 400 g, 4 °C).
Protein concentration was quantified by using the Pierce BCA Protein Assay Kit (23227, Thermo Fisher Scientific). Protein lysates were denatured at 95 °C for 5 min and 20 - 30 µg of protein were generally loaded on polyacrylamide gels and electrophoresis was performed. Separated proteins were transferred onto a PVDF membrane (IPVH00010, Millipore Sigma) by wet-protein transfer. Membranes were blocked in Tris-buffered saline, 0.1% Tween 20 (TBST) containing 5% milk and primary antibodies as listed in Supplementary Table 1 were applied overnight at 4 °C. The secondary, anti-rabbit HRP-conjugated antibody (45-000-682, Thermo Fisher Scientific) was incubated for one hour at RT and bands were visualized using Clarity or Clarity Max Western ECL substrate (1705061 or 1705062, Bio-Rad) with the ChemiDoc™ Imaging System (Bio-Rad).

Immunohistochemistry (IHC)

Tissue designated for IHC analysis was fixed overnight in Z-Fix (NC9050753, Thermo Fisher Scientific), washed with PBS for 30 minutes at RT, processed and embedded in

Downloaded from http://aacrjournals.org/cancerdiscovery/article-pdf/doi/10.1158/2159-8290.CD-24-0137/3472265/cd-24-0137.pdf by Cold Spring Harbor Laboratory user on 15 July 2024

paraffin. The use of human samples was approved by the Henry Ford Health Institutional Review Board. IHC single- and multiplex-staining were performed on 4 µm sections using the Discovery ULTRA stainer (Roche). Antibodies and dilutions are provided in Supplementary Table 1. Hematoxylin and Eosin (H&E) and Picrosirius Red staining were performed according to standard protocols. Stained sections were scanned with the PANNORAMIC SCAN II (3DHistech Ltd.) and the number of positively stained cells / area was quantified with HALO software v3.5.3577.214 (Indica Labs). Representative images were taken from scanned images or with the Stellaris 5 confocal microscope (Leica).

Immunofluorescence (IF)

For IF analysis of adherent pancreatic cancer cells, cells were seeded on chamber slides. Cells were fixed with 4% formaldehyde for 10 minutes at RT, washed with PBS and permeabilized using PBS containing 0.25% Triton X-100 (T8787, Millipore Sigma). After blocking in PBS supplemented with 1% bovine serum albumin (BSA) (BP9703, Thermo Fisher Scientific), 5% donkey serum (D9663, Millipore Sigma) and 0.02% Triton X-100, primary antibodies were incubated overnight at 4°C. Antibodies and dilutions are provided in Supplementary Table 1. Cells were then stained with the secondary antibodies, anti-rabbit 488 (A21206, Thermo Fisher Scientific) and anti-mouse 568 (A10037, Thermo Fisher Scientific) as well as Hoechst 33342 (62249, Thermo Fisher Scientific).

RNA-ISH

Multiplexed RNA-ISH and IF staining were performed as previously described (76). In brief, FFPE sections were baked in a dry air oven at 65°C for one hour, deparaffinized and hydrated in xylene and 100% ethanol. After antigen retrieval in a steamer for 15 minutes using the Co-Detection Target Retrieval (323165, Advanced Cell Diagnostics) solution and blocking, the primary antibody was applied. Slides were post-fixed in 10% Neutral Buffered Formalin (NBF) for 30 minutes at RT and treated with RNAscope®Protease Plus (322381, Advanced Cell Diagnostics) at 40 °C for 11 minutes. For application of RNA-ISH probes, the RNA-ISH Multiplex Fluorescent Assay

Downloaded from http://aacrjournals.org/cancerdiscovery/article-pdf/doi/10.1158/2159-8290.CD-24-0137/3472265/cd-24-0137.pdf by Cold Spring Harbor Laboratory user on 15 July 2024

v2 Kit (323110, Advanced Cell Diagnostics) was used according to manufacturer's instructions. Following RNAscope staining, sections were stained with DAPI at RT for 15 minutes, washed in PBS, secondary antibody was applied and slides were embedded with ProLong Diamond (P36961, Thermo Fisher Scientific) mounting medium.

Single-nucleus ATAC-seq

Pancreatic tissue was snap-frozen in liquid nitrogen and stored at -80 °C. For isolation of nuclei, frozen tissue was pulverized by using the CP02 pulverizer (Covaris). Pulver was washed with PBS containing 0.04% BSA and 1X protease inhibitor and centrifuged (5 min, 500 g, 4 °C). Supernatant was discarded, pellet was resuspended in 0.1 U/µl DNase solution (EN0521, Thermo Fisher Scientific) and incubated on ice for 5 minutes. Tissue was washed twice with PBS containing 0.04% BSA and 1X protease inhibitor. After the last centrifugation step (5 min, 500 g, 4 °C), supernatant was discarded, pellet was resuspended in freshly prepared lysis buffer (10 mM Tris-HCl, 10 mM NaCl, 3 mM $MgCl_2$, 0.1% Tween-20, 0.1% Nonident P40, 0.01% Digitonin (BN2006, Thermo Fisher Scientific), 1% BSA and 1X protease inhibitor) and incubated on ice for 10 minutes. Then, nuclei were isolated by using a 2 ml Dounce homogenizer, 25 strokes with pestle A and 25 strokes with pestle B. To remove connective tissue and residual debris, sample was filtrated through a 70 µm cell strainer (352350, Thermo Fisher Scientific), followed by centrifugation (1 min, 100 g, 4 °C). Supernatant was transferred to a new tube and washed with wash buffer (10 mM Tris-HCl, 10 mM NaCl, 3 mM $MgCl_2$, 0.1% Tween-20, 1% BSA and 1X protease inhibitor) followed by centrifugation (5 min, 500 g, 4°C) for three times. Before the final washing step, suspension was filtered through a 40 µm Flowmi cell strainer (BAH136800040-50EA, Millipore Sigma). Finally, nuclei were resuspended in Nuclei Buffer (10X Genomics). Library preparation and sequencing was performed at the Advanced Genomics Core of the University of Michigan. First, single nucleus suspensions were counted on the LUNA Fx7 Automated Cell Counter (Logos Biosystems). Then, single nucleus ATAC libraries were generated using the 10x Genomics Chromium instrument following the manufacturer's protocol. Final library quality was assessed using the LabChip GX (PerkinElmer). Pooled libraries were

Downloaded from http://aacrjournals.org/cancerdiscovery/article-pdf/doi/10.1158/2159-8290.CD-24-0137/3472265/cd-24-0137.pdf by Cold Spring Harbor Laboratory user on 15 July 2024

subjected to paired-end sequencing according to the manufacturer's protocol (Illumina NovaSeq 6000). 10,000 cells were profiled with a sequencing depth of 50,000 reads per cell. Bcl2fastq2 Conversion Software (Illumina) was used to generate demultiplexed fastq files. Raw sequencing data was processed using cellranger-atac-2.0.0 (10X Genomics) and reads were aligned to mm10 reference genome.

Single-nucleus ATAC-seq Data Processing

Doublet removal was performed using scDblFinder (excluding cells with a $-\log_{10}$(q-value)) (77) and AMULET (doublet score > 0.975) (78). In addition, nuclei were excluded if number of reads with low mapping quality was > 40,000, percent of mitochondrial reads was > 10%, percentage of reads in peaks was < 20%, nucleosome signal was > 0.63, activity was detectable in < 3,200 features or > 32,000 features and TSS enrichment score < 2.5. Next, features with < 500 counts across all samples or with reads in < 1% of cells were excluded. Gene activity scores and features were created using the GeneActivity function from the Signac R package (29). Genes with an activity score of < 200 across all cells (per-sample) or with activity scores in < 1% of cells (per-sample) as well as nuclei with activity scores in < 1,000 genes were removed. For each nucleus, gene activity scores were normalized and natural log transformed. Uniform Manifold Approximation and Projection (UMAP) and shared nearest-neighbor graph (SNN) were constructed using the Seurat R packages RunUMAP and FindNeighbors functions, respectively (79). Dimensional reduction was performed via latent semantic indexing (lsi) using dimensions 2:30. Cell clusters were identified using the FindClusters function with smart local moving (SLM) algorithm (resolution=0.4) (80). UMAP projection created a central cluster of low-quality nuclei that demonstrated comparatively poorer QC metrics, such as significantly lower percentage of reads in peaks, lower TSS enrichment and mapping quality scores. This cluster as well as clusters with < 20 cells were removed. Due to a lymph node contamination in one of the two-week snATAC-seq samples, sequencing of one sample was repeated. The minor batch effect was remedied via ComBat (81) using adjusted cluster labels in the model matrix. UMAP projects were recreated with batch-corrected data as described above. The Seurat R package FindAllMarkers function was used to identify differentially accessible peaks

Downloaded from http://aacrjournals.org/cancerdiscovery/article-pdf/doi/10.1158/2159-8290.CD-24-0137/3472265/cd-24-0137.pdf by Cold Spring Harbor Laboratory user on 15 July 2024

among cell clusters (79). Potential marker genes were required to be present in at least 25% of cells per cluster and show on average, at least a 0.25-fold difference (log-scale) among cell populations. Based on identified cluster-specific marker genes, clusters were manually annotated.

RNA Isolation and Quantitative Real-time PCR (qRT-PCR)

For total RNA extraction, the RNeasy® Plus Mini Kit (74134, Qiagen) was used following manufacturer's instructions. Genomic DNA was digested on column by using the RNase-Free DNase Set (79254, Qiagen). mRNA was reverse transcribed to cDNA with the iScript(tm) cDNA Synthesis Kit (1708891BUN, Bio-Rad). qRT-PCR was performed on the QuantStudio 6 Pro qRT-PCR cycler (Thermo Fisher Scientific) using 20 ng cDNA, 500 nM forward and reverse primers as well as 1X Fast SYBR Green Master Mix per reaction (4385612, Thermo Fisher Scientific). Primer sequences are provided in Supplementary Table 2. Relative gene expression was determined in relation to expression of the housekeeping genes *GAPDH* and *Hprt1* and calculated according to the ΔΔCt method (82).

Bulk RNA-seq

Total RNA was at least analyzed in triplicates. Library preparation and sequencing of RNA samples from isolated mouse acinar cells were performed at the University of Michigan Advanced Genomics Core. Libraries underwent paired-end sequencing with 37.5M reads per sample. Human RNA samples were processed at MedGenome Inc. RNA-seq library preparation was performed by using the Illumina TruSeq stranded mRNA kit. RNA-seq libraries were paired-end sequenced (PE100/150) with 40M reads per sample.

Bulk RNA-seq Data Processing

Sequencing reads of mouse RNA-seq experiments from isolated acinar cells were assessed for quality and quantity metrics using FastQC and multiQC (83). Reads were aligned to the mouse reference genome (GRCm38/mm10 Ensembl release 98) using Salmon (84). Sample-specific transcripts per kilobase million (TPM) estimates were

Downloaded from http://aacrjournals.org/cancerdiscovery/article-pdf/doi/10.1158/2159-8290.CD-24-0137/3472265/cd-24-0137.pdf by Cold Spring Harbor Laboratory user on 15 July 2024

manually converted to gene-specific TPM estimates by summing transcript TPMs per gene. Genes and their respective transcripts were collected using the tr2g_ensembl function from the BUSpaRse R package. The original sample by gene count matrix (TPM) was first adjusted for per-sample sequencing library inspired by DESeq2 (85). The geometric mean was calculated for each gene across all samples. Gene counts were divided by this geometric mean, resulting in gene count ratios. A sample-specific-median or “sample size factor” of these ratios was finally divided from each gene count per sample. Features with estimates < 1 TPM were removed, gene counts were $\log_2$ transformed and the top 2,000 most variable genes were selected. The gene expression matrix was further normalized by centering and scaling for each gene using (E-mean(E)/sd(E)). For unsupervised clustering of these genes the geometric means of the normalized counts per treatment group were used. Cluster analysis was performed using the Self-Organizing Map Program Package (SOM PAK) (version 3.1) (86).

For RNA-seq experiments of human pancreatic cancer cell lines, adapter trimming and removal of ribosomal and mitochondrial genome was carried out with fastq-mcf, cutadapt and Bowtie2 (87), respectively. Reads were mapped to the hg19 genome using STAR (88) and raw read counts were estimated with HTSeq (v0.11.2) (89) and normalized with DESeq2 (85).

Pseudo Bulk ATAC- and RNA-seq (Bi-Omic) Cross-correlation Analysis

In order to compare the snATAC-seq data to bulk RNA-seq data of isolated acinar cells, a sample by gene *pseudo-bulk* count matrix was created. First, UMAP clusters identified as acinar cells were subset from the snATAC-seq Seurat object. Then, acinar cells were grouped by sample and the trimmed arithmetic mean of raw counts was calculated to represent the *pseudo bulk* counts; a fraction of 0.05 of observations was trimmed from each end of per-gene counts before the mean was computed. The *pseudo-bulk* sample by gene read count matrix (8x20227) was adjusted for per-sample sequencing library inspired by DESeq2 (85) and calculated as described above. Genes with < 1 count across all samples were removed, gene counts were $\log_2$ transformed and the top 2000 most variable genes were selected. The *pseudo-bulk* ATAC-seq sample-by-gene (8x2000) transformed count matrix was compared to the RNA-Seq sample-by-gene

Downloaded from http://aacrjournals.org/cancerdiscovery/article-pdf/doi/10.1158/2159-8290.CD-24-0137/3472265/cd-24-0137.pdf by Cold Spring Harbor Laboratory user on 15 July 2024

(12x2000) transformed count matrix. Both matrices were adjusted for per-sample sequencing library and $\log_2$ transformed. Any missing values were imputed with a value of zero. After performing a sample-by-sample spearman correlation and a principal component analysis on the 374 shared genes across the 12 samples of the RNA-seq matrix (biological replicates per genotype n=3), the most distant samples per experimental condition were removed. Both matrices including a total of 8 samples were then standardized by centering and scaling for each gene using (E-mean(E))/sd(E). ATAC-seq genes were measured for their correlation (Spearman) to their respective RNA-seq genes. Genes that demonstrated a correlation ≥ 0.5 were subset (n=117).

Analysis of Publicly Available Transcriptome Datasets

Single-cell gene expression data from mouse pancreas cells were downloaded from Gene Expression Omnibus (GEO) (GSE141017, Samples GSM4293545-GSM4293554) (19). Scanpy version 1.9.3 (90) was used for re-processing of the digital count matrixes. Counts were normalized to a target sum of 10,000 after masking highly expressed genes, log-transformed, scaled, and the first 50 principal components were used for Leiden clustering and UMAP projection. The PCA space was batch corrected using Harmony (91) with the sample batch as a covariate and the diversity clustering penalty parameter (theta) = 4, and otherwise default settings. Coarse clustering was achieved with a low Leiden resolution score (0.1), and epithelial cell types were selected after screening clusters for expression of the following marker genes: epithelial (*Krt8*, *Krt18*, *Krt19*), endothelial (*Cdh5*, *Pecam1*, *Plvap*), mesenchymal (*Col3a1*, *Dcn*, *Sparc*) and immune (*Tyrobp*, *Cd52*, *Ptprc*). Samples were then re-processed with the same settings as above. Epithelial cells were again coarsely clustered, and the primary acinar cell cluster was distinguished from ductal-type cells by the presence of exocrine marker genes (*Ctrb1, Prss2, Try5*). Meta/neoplastic cells were identified by tdTomato expression. In brief, K-means (K=2, scikit-learn v1.2.2) clustering was carried out on the log-normalized tdTomato expression levels across all epithelial cells. Cells in the higher expression group that were not present in the predominant acinar cell cluster were assigned as meta/neoplastic cells. To calculate cell type scores, gene lists were

Downloaded from http://aacrjournals.org/cancerdiscovery/article-pdf/doi/10.1158/2159-8290.CD-24-0137/3472265/cd-24-0137.pdf by Cold Spring Harbor Laboratory user on 15 July 2024

compiled from Busslinger et al. (34) and scored using the Scanpy function scanpy.tl.score_genes().

Single-cell gene expression data from mouse stomach cells were downloaded from GEO (GSE141017, Sample GSM4293556) (19). Samples were processed as described above, except that coarse clustering was achieved with a resolution score of 0.04 and cells with < 3,000 UMIs were removed.

For the reanalysis of injury-induced ADM dataset (Ma et al.: GSE172380) (21), all YFP+ cells (GSE172380_Cluster+CelltypeLabel_YFP+_all-samples_QCed.csv.gz) were processed with Scanpy using the same pipeline, except cells with < 1,000 UMIs or > 20% mitochondrial content were discarded.

For analyzing RNA-seq data from mouse PDAC cell lines, data (GSE107458) (42) were downloaded from GEO and aligned to mm10. Quality control and normalization was performed and normalized matrix was subjected to Pearson's correlation to assess correlation of *Ror2* to the expression of other genes. Top 50 positively and negatively correlated genes were selected for further analysis and a heatmap depicting mean normalized expression values was generated using pheatmap. Distribution of normalized expression for candidate markers genes with respect to *Ror2* were plotted. Moreover, expression of top 50 most significantly enriched genes in pit cell-like ADM from Schlesinger et al. (19) data was visualized in a heatmap.

To analyze previously published RNA-seq data of human PDAC samples (GSE93326) (52), processed data were retrieved from GEO and counts were normalized using the normTransform function from DESeq2. Only micro-dissected tumor samples were selected for further analysis. For PDAC tumor subtype annotation, Moffitt's (23) top-25 gene signature was employed and clustering was performed using ConsensusClusterPlus. Correlation analysis was performed as described above. Analyses were performed using R (version 4.3.1).

For the analysis of human PDAC scRNA-seq data, samples from 174 primary tumors were included (EGAS00001002543, GSE154778, GSE155698, GSE156405, GSE194247, GSE202051, GSE205013, GSE211644, phs001840.v1.p1, PRJCA001063) (2,43-51). Post quality control and data harmonization was performed using Harmony (91) and ductal cells based on expression levels of *KRT18* and *KRT19*

Downloaded from http://aacrjournals.org/cancerdiscovery/article-pdf/doi/10.1158/2159-8290.CD-24-0137/3472265/cd-24-0137.pdf by Cold Spring Harbor Laboratory user on 15 July 2024

were selected for further analysis. Using single sample gene set enrichment (ssGSEA) (92), each cell was scored for the expression of previously defined classical, basal-like, intermediate (27) and the established pit cell-like ADM signature (50 genes). Cell specific scores were converted to z-scores for comparison between signatures and cell clusters were classified according to their signatures. Using Pearson's correlation, the correlations between the classical and pit cell-like ADM signature as well as the basal-like cell and pit cell-like ADM signature were assessed.

Functional Annotation of Bulk RNA-seq Data

GSEA (Gene Set Enrichment Analysis) was performed using the GSEA software 4.3.2 (93). For analysis of mouse RNA-seq data, normalized read counts that were centered and scaled by feature were used as input and enrichment analysis was run for generated SPEM signature gene set. GSEA for human cell line RNA-seq data was performed with normalized read counts and data were aligned to the H: hallmark gene sets. Pathway analysis were performed using the Database for Annotation, Visualization and Integrated Discovery (DAVID) (94,95). For the generation of GO terms, genes that exhibited a Pearson correlation coefficient > 0.4 and < -0.4, and a p-value <0.01 were used. EMT score was calculated based on $\log_2$ normalized read counts by using a custom-built function (https://github.com/umahajanatlmu/useful_commands/blob/main/EMT_signature_score.R) incorporating gene signatures from a meta-analysis of 18 independent gene expression studies (53).

Quantification and Statistical Analysis

Statistical significance was calculated by two-tailed, unpaired Student's *t*-test and Mann-Whitney U test as indicated; * $p < 0.05$, ** $p < 0.01$, *** $p < 0.001$, **** $p < 0.0001$. Statistical analysis was performed with GraphPad Prism 9 software (GraphPad Software Inc.).

Data Availability

Downloaded from http://aacrjournals.org/cancerdiscovery/article-pdf/doi/10.1158/2159-8290.CD-24-0137/3472265/cd-24-0137.pdf by Cold Spring Harbor Laboratory user on 15 July 2024

The sequencing data generated in this study have been deposited on Gene Expression Omnibus (GEO) database and are accessible through GEO Series accession number GSE253600.

Downloaded from http://aacrjournals.org/cancerdiscovery/article-pdf/doi/10.1158/2159-8290.CD-24-0137/3472265/cd-24-0137.pdf by Cold Spring Harbor Laboratory user on 15 July 2024

Acknowledgments

The authors would like to thank the University of Michigan Epigenomics Core and Advanced Genomics Core for tissue preparation and sequencing services, respectively. We would like to thank Dr. Ethan Abel for providing packaging plasmids. We would like to thank Drs. Linda C. Samuelson, Samantha Kemp and Stephen Parker for the helpful discussions. This work was supported in part by Michigan State University through computational resources provided by the Institute for Cyber-Enabled Research (ICER). This work was supported by R01CA247516, U01CA224145 and U01CA274154 (to Howard C. Crawford). Simone Benitz was supported by a postdoctoral fellowship from the German Research Foundation (BE 7224/1-1) and a research grant provided by the Sky Foundation. Ujjwal Mukund Mahajan was supported by the German Research Foundation (MA 4115/3-1) and the German Cancer Aid (70115409). Daniel J. Salas-Escabillas was supported by 1F31CA271576. Nina G. Steele was supported by R00CA263154.

References

1. Aung KL, Fischer SE, Denroche RE, Jang GH, Dodd A, Creighton S*, et al.* Genomics-Driven Precision Medicine for Advanced Pancreatic Cancer: Early Results from the COMPASS Trial. Clin Cancer Res **2018**;24(6):1344-54 doi 10.1158/1078-0432.CCR-17-2994.
2. Werba G, Weissinger D, Kawaler EA, Zhao E, Kalfakakou D, Dhara S*, et al.* Single-cell RNA sequencing reveals the effects of chemotherapy on human pancreatic adenocarcinoma and its tumor microenvironment. Nat Commun **2023**;14(1):797 doi 10.1038/s41467-023-36296-4.
3. O'Kane GM, Grunwald BT, Jang GH, Masoomian M, Picardo S, Grant RC*, et al.* GATA6 Expression Distinguishes Classical and Basal-like Subtypes in Advanced

Pancreatic Cancer. Clin Cancer Res **2020**;26(18):4901-10 doi 10.1158/1078-0432.CCR-19-3724.
4. Krebs AM, Mitschke J, Lasierra Losada M, Schmalhofer O, Boerries M, Busch H*, et al.* The EMT-activator Zeb1 is a key factor for cell plasticity and promotes metastasis in pancreatic cancer. Nat Cell Biol **2017**;19(5):518-29 doi 10.1038/ncb3513.
5. Shields MA, Ebine K, Sahai V, Kumar K, Siddiqui K, Hwang RF*, et al.* Snail cooperates with KrasG12D to promote pancreatic fibrosis. Mol Cancer Res **2013**;11(9):1078-87 doi 10.1158/1541-7786.MCR-12-0637.
6. Habbe N, Shi G, Meguid RA, Fendrich V, Esni F, Chen H*, et al.* Spontaneous induction of murine pancreatic intraepithelial neoplasia (mPanIN) by acinar cell targeting of oncogenic Kras in adult mice. Proc Natl Acad Sci U S A **2008**;105(48):18913-8 doi 10.1073/pnas.0810097105.
7. Strobel O, Dor Y, Alsina J, Stirman A, Lauwers G, Trainor A*, et al.* In vivo lineage tracing defines the role of acinar-to-ductal transdifferentiation in inflammatory ductal metaplasia. Gastroenterology **2007**;133(6):1999-2009 doi 10.1053/j.gastro.2007.09.009.
8. Kopp JL, von Figura G, Mayes E, Liu FF, Dubois CL, Morris JPt*, et al.* Identification of Sox9-dependent acinar-to-ductal reprogramming as the principal mechanism for initiation of pancreatic ductal adenocarcinoma. Cancer Cell **2012**;22(6):737-50 doi 10.1016/j.ccr.2012.10.025.
9. Lo EKW, Mears BM, Maurer HC, Idrizi A, Hansen KD, Thompson ED*, et al.* Comprehensive DNA Methylation Analysis Indicates That Pancreatic Intraepithelial Neoplasia Lesions Are Acinar-Derived and Epigenetically Primed for Carcinogenesis. Cancer Res **2023**;83(11):1905-16 doi 10.1158/0008-5472.CAN-22-4052.
10. Guerra C, Schuhmacher AJ, Canamero M, Grippo PJ, Verdaguer L, Perez-Gallego L*, et al.* Chronic pancreatitis is essential for induction of pancreatic ductal adenocarcinoma by K-Ras oncogenes in adult mice. Cancer Cell **2007**;11(3):291-302 doi 10.1016/j.ccr.2007.01.012.
11. Jensen JN, Cameron E, Garay MV, Starkey TW, Gianani R, Jensen J. Recapitulation of elements of embryonic development in adult mouse pancreatic regeneration. Gastroenterology **2005**;128(3):728-41 doi 10.1053/j.gastro.2004.12.008.
12. Zhong B, Zhou Q, Toivola DM, Tao GZ, Resurreccion EZ, Omary MB. Organ-specific stress induces mouse pancreatic keratin overexpression in association with NF-kappaB activation. J Cell Sci **2004**;117(Pt 9):1709-19 doi 10.1242/jcs.01016.
13. Kalisz M, Bernardo E, Beucher A, Maestro MA, Del Pozo N, Millan I*, et al.* HNF1A recruits KDM6A to activate differentiated acinar cell programs that suppress pancreatic cancer. EMBO J **2020**;39(9):e102808 doi 10.15252/embj.2019102808.
14. Cobo I, Martinelli P, Flandez M, Bakiri L, Zhang M, Carrillo-de-Santa-Pau E*, et al.* Transcriptional regulation by NR5A2 links differentiation and inflammation in the pancreas. Nature **2018**;554(7693):533-7 doi 10.1038/nature25751.

Downloaded from http://aacrjournals.org/cancerdiscovery/article-pdf/doi/10.1158/2159-8290.CD-24-0137/3472265/cd-24-0137.pdf by Cold Spring Harbor Laboratory user on 15 July 2024

15. Shi G, Zhu L, Sun Y, Bettencourt R, Damsz B, Hruban RH*, et al.* Loss of the acinar-restricted transcription factor Mist1 accelerates Kras-induced pancreatic intraepithelial neoplasia. Gastroenterology **2009**;136(4):1368-78 doi 10.1053/j.gastro.2008.12.066.
16. Krah NM, De La OJ, Swift GH, Hoang CQ, Willet SG, Chen Pan F*, et al.* The acinar differentiation determinant PTF1A inhibits initiation of pancreatic ductal adenocarcinoma. Elife **2015**;4 doi 10.7554/eLife.07125.
17. Roy N, Takeuchi KK, Ruggeri JM, Bailey P, Chang D, Li J*, et al.* PDX1 dynamically regulates pancreatic ductal adenocarcinoma initiation and maintenance. Genes Dev **2016**;30(24):2669-83 doi 10.1101/gad.291021.116.
18. Li D, Duell EJ, Yu K, Risch HA, Olson SH, Kooperberg C*, et al.* Pathway analysis of genome-wide association study data highlights pancreatic development genes as susceptibility factors for pancreatic cancer. Carcinogenesis **2012**;33(7):1384-90 doi 10.1093/carcin/bgs151.
19. Schlesinger Y, Yosefov-Levi O, Kolodkin-Gal D, Granit RZ, Peters L, Kalifa R*, et al.* Single-cell transcriptomes of pancreatic preinvasive lesions and cancer reveal acinar metaplastic cells' heterogeneity. Nat Commun **2020**;11(1):4516 doi 10.1038/s41467-020-18207-z.
20. Willet SG, Mills JC. Stomach Organ and Cell Lineage Differentiation: from Embryogenesis to Adult Homeostasis. Cell Mol Gastroenterol Hepatol **2016**;2(5):546-59 doi 10.1016/j.jcmgh.2016.05.006.
21. Ma Z, Lytle NK, Chen B, Jyotsana N, Novak SW, Cho CJ*, et al.* Single-Cell Transcriptomics Reveals a Conserved Metaplasia Program in Pancreatic Injury. Gastroenterology **2022**;162(2):604-20 e20 doi 10.1053/j.gastro.2021.10.027.
22. Goldenring JR, Mills JC. Cellular Plasticity, Reprogramming, and Regeneration: Metaplasia in the Stomach and Beyond. Gastroenterology **2022**;162(2):415-30 doi 10.1053/j.gastro.2021.10.036.
23. Moffitt RA, Marayati R, Flate EL, Volmar KE, Loeza SG, Hoadley KA*, et al.* Virtual microdissection identifies distinct tumor- and stroma-specific subtypes of pancreatic ductal adenocarcinoma. Nat Genet **2015**;47(10):1168-78 doi 10.1038/ng.3398.
24. Collisson EA, Sadanandam A, Olson P, Gibb WJ, Truitt M, Gu S*, et al.* Subtypes of pancreatic ductal adenocarcinoma and their differing responses to therapy. Nat Med **2011**;17(4):500-3 doi 10.1038/nm.2344.
25. Bailey P, Chang DK, Nones K, Johns AL, Patch AM, Gingras MC*, et al.* Genomic analyses identify molecular subtypes of pancreatic cancer. Nature **2016**;531(7592):47-52 doi 10.1038/nature16965.
26. Williams HL, Dias Costa A, Zhang J, Raghavan S, Winter PS, Kapner KS*, et al.* Spatially Resolved Single-Cell Assessment of Pancreatic Cancer Expression Subtypes Reveals Co-expressor Phenotypes and Extensive Intratumoral Heterogeneity. Cancer Res **2023**;83(3):441-55 doi 10.1158/0008-5472.CAN-22-3050.
27. Raghavan S, Winter PS, Navia AW, Williams HL, DenAdel A, Lowder KE*, et al.* Microenvironment drives cell state, plasticity, and drug response in pancreatic cancer. Cell **2021**;184(25):6119-37 e26 doi 10.1016/j.cell.2021.11.017.

Downloaded from http://aacrjournals.org/cancerdiscovery/article-pdf/doi/10.1158/2159-8290.CD-24-0137/3472265/cd-24-0137.pdf by Cold Spring Harbor Laboratory user on 15 July 2024

28. Benitz S, Straub T, Mahajan UM, Mutter J, Czemmel S, Unruh T*, et al.* Ring1b-dependent epigenetic remodelling is an essential prerequisite for pancreatic carcinogenesis. Gut **2019**;68(11):2007-18 doi 10.1136/gutjnl-2018-317208.
29. Stuart T, Srivastava A, Madad S, Lareau CA, Satija R. Single-cell chromatin state analysis with Signac. Nat Methods **2021**;18(11):1333-41 doi 10.1038/s41592-021-01282-5.
30. Tu M, Klein L, Espinet E, Georgomanolis T, Wegwitz F, Li X*, et al.* TNF-alpha-producing macrophages determine subtype identity and prognosis via AP1 enhancer reprogramming in pancreatic cancer. Nat Cancer **2021**;2(11):1185-203 doi 10.1038/s43018-021-00258-w.
31. Menck K, Heinrichs S, Wlochowitz D, Sitte M, Noeding H, Janshoff A*, et al.* WNT11/ROR2 signaling is associated with tumor invasion and poor survival in breast cancer. J Exp Clin Cancer Res **2021**;40(1):395 doi 10.1186/s13046-021-02187-z.
32. Castro MV, Barbero GA, Mascolo P, Villanueva MB, Nsengimana J, Newton-Bishop J*, et al.* ROR2 promotes epithelial-mesenchymal transition by hyperactivating ERK in melanoma. J Cell Commun Signal **2023**;17(1):75-88 doi 10.1007/s12079-022-00683-1.
33. O'Connell MP, Fiori JL, Xu M, Carter AD, Frank BP, Camilli TC*, et al.* The orphan tyrosine kinase receptor, ROR2, mediates Wnt5A signaling in metastatic melanoma. Oncogene **2010**;29(1):34-44 doi 10.1038/onc.2009.305.
34. Busslinger GA, Weusten BLA, Bogte A, Begthel H, Brosens LAA, Clevers H. Human gastrointestinal epithelia of the esophagus, stomach, and duodenum resolved at single-cell resolution. Cell Rep **2021**;34(10):108819 doi 10.1016/j.celrep.2021.108819.
35. Takada H, Sasagawa Y, Yoshimura M, Tanaka K, Iwayama Y, Hayashi T*, et al.* Single-cell transcriptomics uncovers EGFR signaling-mediated gastric progenitor cell differentiation in stomach homeostasis. Nat Commun **2023**;14(1):3750 doi 10.1038/s41467-023-39113-0.
36. Prasad NB, Biankin AV, Fukushima N, Maitra A, Dhara S, Elkahloun AG*, et al.* Gene expression profiles in pancreatic intraepithelial neoplasia reflect the effects of Hedgehog signaling on pancreatic ductal epithelial cells. Cancer Res **2005**;65(5):1619-26 doi 10.1158/0008-5472.CAN-04-1413.
37. Bockerstett KA, Lewis SA, Wolf KJ, Noto CN, Jackson NM, Ford EL*, et al.* Single-cell transcriptional analyses of spasmolytic polypeptide-expressing metaplasia arising from acute drug injury and chronic inflammation in the stomach. Gut **2020**;69(6):1027-38 doi 10.1136/gutjnl-2019-318930.
38. Weis VG, Sousa JF, LaFleur BJ, Nam KT, Weis JA, Finke PE*, et al.* Heterogeneity in mouse spasmolytic polypeptide-expressing metaplasia lineages identifies markers of metaplastic progression. Gut **2013**;62(9):1270-9 doi 10.1136/gutjnl-2012-302401.
39. Engevik AC, Feng R, Choi E, White S, Bertaux-Skeirik N, Li J*, et al.* The Development of Spasmolytic Polypeptide/TFF2-Expressing Metaplasia (SPEM) During Gastric Repair Is Absent in the Aged Stomach. Cell Mol Gastroenterol Hepatol **2016**;2(5):605-24 doi 10.1016/j.jcmgh.2016.05.004.

Downloaded from http://aacrjournals.org/cancerdiscovery/article-pdf/doi/10.1158/2159-8290.CD-24-0137/3472265/cd-24-0137.pdf by Cold Spring Harbor Laboratory user on 15 July 2024

40. Si H, Zhao N, Pedroza A, Zaske AM, Rosen JM, Creighton CJ*, et al.* Noncanonical Wnt/Ror2 signaling regulates cell-matrix adhesion to prompt directional tumor cell invasion in breast cancer. Mol Biol Cell **2022**;33(11):ar103 doi 10.1091/mbc.E22-02-0055.
41. Aiello NM, Maddipati R, Norgard RJ, Balli D, Li J, Yuan S*, et al.* EMT Subtype Influences Epithelial Plasticity and Mode of Cell Migration. Dev Cell **2018**;45(6):681-95 e4 doi 10.1016/j.devcel.2018.05.027.
42. Mueller S, Engleitner T, Maresch R, Zukowska M, Lange S, Kaltenbacher T*, et al.* Evolutionary routes and KRAS dosage define pancreatic cancer phenotypes. Nature **2018**;554(7690):62-8 doi 10.1038/nature25459.
43. Chan-Seng-Yue M, Kim JC, Wilson GW, Ng K, Figueroa EF, O'Kane GM*, et al.* Transcription phenotypes of pancreatic cancer are driven by genomic events during tumor evolution. Nat Genet **2020**;52(2):231-40 doi 10.1038/s41588-019-0566-9.
44. Lin W, Noel P, Borazanci EH, Lee J, Amini A, Han IW*, et al.* Single-cell transcriptome analysis of tumor and stromal compartments of pancreatic ductal adenocarcinoma primary tumors and metastatic lesions. Genome Med **2020**;12(1):80 doi 10.1186/s13073-020-00776-9.
45. Steele NG, Carpenter ES, Kemp SB, Sirihorachai VR, The S, Delrosario L*, et al.* Multimodal Mapping of the Tumor and Peripheral Blood Immune Landscape in Human Pancreatic Cancer. Nat Cancer **2020**;1(11):1097-112 doi 10.1038/s43018-020-00121-4.
46. Lee JJ, Bernard V, Semaan A, Monberg ME, Huang J, Stephens BM*, et al.* Elucidation of Tumor-Stromal Heterogeneity and the Ligand-Receptor Interactome by Single-Cell Transcriptomics in Real-world Pancreatic Cancer Biopsies. Clin Cancer Res **2021**;27(21):5912-21 doi 10.1158/1078-0432.CCR-20-3925.
47. Elyada E, Bolisetty M, Laise P, Flynn WF, Courtois ET, Burkhart RA*, et al.* Cross-Species Single-Cell Analysis of Pancreatic Ductal Adenocarcinoma Reveals Antigen-Presenting Cancer-Associated Fibroblasts. Cancer Discov **2019**;9(8):1102-23 doi 10.1158/2159-8290.CD-19-0094.
48. Peng J, Sun BF, Chen CY, Zhou JY, Chen YS, Chen H*, et al.* Single-cell RNA-seq highlights intra-tumoral heterogeneity and malignant progression in pancreatic ductal adenocarcinoma. Cell Res **2019**;29(9):725-38 doi 10.1038/s41422-019-0195-y.
49. Hwang WL, Jagadeesh KA, Guo JA, Hoffman HI, Yadollahpour P, Reeves JW*, et al.* Single-nucleus and spatial transcriptome profiling of pancreatic cancer identifies multicellular dynamics associated with neoadjuvant treatment. Nat Genet **2022**;54(8):1178-91 doi 10.1038/s41588-022-01134-8.
50. Shiau C, Su J, Guo JA, Hong TS, Wo JY, Jagadeesh KA*, et al.* Treatment-associated remodeling of the pancreatic cancer endothelium at single-cell resolution. Front Oncol **2022**;12:929950 doi 10.3389/fonc.2022.929950.
51. Schalck A, Sakellariou-Thompson D, Forget MA, Sei E, Hughes TG, Reuben A*, et al.* Single-Cell Sequencing Reveals Trajectory of Tumor-Infiltrating Lymphocyte States in Pancreatic Cancer. Cancer Discov **2022**;12(10):2330-49 doi 10.1158/2159-8290.CD-21-1248.

Downloaded from http://aacrjournals.org/cancerdiscovery/article-pdf/doi/10.1158/2159-8290.CD-24-0137/3472265/cd-24-0137.pdf by Cold Spring Harbor Laboratory user on 15 July 2024

52. Maurer C, Holmstrom SR, He J, Laise P, Su T, Ahmed A*, et al.* Experimental microdissection enables functional harmonisation of pancreatic cancer subtypes. Gut **2019**;68(6):1034-43 doi 10.1136/gutjnl-2018-317706.
53. Groger CJ, Grubinger M, Waldhor T, Vierlinger K, Mikulits W. Meta-analysis of gene expression signatures defining the epithelial to mesenchymal transition during cancer progression. PLoS One **2012**;7(12):e51136 doi 10.1371/journal.pone.0051136.
54. Mani SA, Guo W, Liao MJ, Eaton EN, Ayyanan A, Zhou AY*, et al.* The epithelial-mesenchymal transition generates cells with properties of stem cells. Cell **2008**;133(4):704-15 doi 10.1016/j.cell.2008.03.027.
55. Perez G, Lopez-Moncada F, Indo S, Torres MJ, Castellon EA, Contreras HR. Knockdown of ZEB1 reverses cancer stem cell properties in prostate cancer cells. Oncol Rep **2021**;45(5) doi 10.3892/or.2021.8009.
56. Sanada M, Yamazaki M, Yamada T, Fujino K, Kudoh S, Tenjin Y*, et al.* Heterogeneous expression and role of receptor tyrosine kinase-like orphan receptor 2 (ROR2) in small cell lung cancer. Hum Cell **2023**;36(1):409-20 doi 10.1007/s13577-022-00830-1.
57. Avincsal MO, Kamizaki K, Jimbo N, Shinomiya H, Nibu KI, Nishita M*, et al.* Oncogenic E6 and/or E7 proteins drive proliferation and invasion of human papilloma virus-positive head and neck squamous cell cancer through upregulation of Ror2 expression. Oncol Rep **2021**;46(1) doi 10.3892/or.2021.8099.
58. Flowers BM, Xu H, Mulligan AS, Hanson KJ, Seoane JA, Vogel H*, et al.* Cell of Origin Influences Pancreatic Cancer Subtype. Cancer Discov **2021**;11(3):660-77 doi 10.1158/2159-8290.CD-20-0633.
59. Hoang CQ, Hale MA, Azevedo-Pouly AC, Elsasser HP, Deering TG, Willet SG*, et al.* Transcriptional Maintenance of Pancreatic Acinar Identity, Differentiation, and Homeostasis by PTF1A. Mol Cell Biol **2016**;36(24):3033-47 doi 10.1128/MCB.00358-16.
60. Cephas AT, Hwang WL, Maitra A, Parnas O, DelGiorno KE. It is better to light a candle than to curse the darkness: single-cell transcriptomics sheds new light on pancreas biology and disease. Gut **2023**;72(6):1211-9 doi 10.1136/gutjnl-2022-329313.
61. Shi ZD, Pang K, Wu ZX, Dong Y, Hao L, Qin JX*, et al.* Tumor cell plasticity in targeted therapy-induced resistance: mechanisms and new strategies. Signal Transduct Target Ther **2023**;8(1):113 doi 10.1038/s41392-023-01383-x.
62. Ge X, Lin F, Wu Z, Lin Y, Tang W, McKay MJ*, et al.* Role of ROR2 in promoting gastric cancer metastasis by enhancing c-JUN-mediated MMP3 transcription. Ann Transl Med **2022**;10(20):1117 doi 10.21037/atm-22-4583.
63. Bland T, Wang J, Yin L, Pu T, Li J, Gao J*, et al.* WLS-Wnt signaling promotes neuroendocrine prostate cancer. iScience **2021**;24(1):101970 doi 10.1016/j.isci.2020.101970.
64. Castro MV, Barbero GA, Mascolo P, Ramos R, Quezada MJ, Lopez-Bergami P. ROR2 increases the chemoresistance of melanoma by regulating p53 and Bcl2-family proteins via ERK hyperactivation. Cell Mol Biol Lett **2022**;27(1):23 doi 10.1186/s11658-022-00327-7.

Downloaded from http://aacrjournals.org/cancerdiscovery/article-pdf/doi/10.1158/2159-8290.CD-24-0137/3472265/cd-24-0137.pdf by Cold Spring Harbor Laboratory user on 15 July 2024

65. O'Connell MP, Marchbank K, Webster MR, Valiga AA, Kaur A, Vultur A*, et al.* Hypoxia induces phenotypic plasticity and therapy resistance in melanoma via the tyrosine kinase receptors ROR1 and ROR2. Cancer Discov **2013**;3(12):1378-93 doi 10.1158/2159-8290.CD-13-0005.
66. Dai B, Yan T, Zhang A. ROR2 receptor promotes the migration of osteosarcoma cells in response to Wnt5a. Cancer Cell Int **2017**;17:112 doi 10.1186/s12935-017-0482-y.
67. Bordonaro M, Tewari S, Cicco CE, Atamna W, Lazarova DL. A switch from canonical to noncanonical Wnt signaling mediates drug resistance in colon cancer cells. PLoS One **2011**;6(11):e27308 doi 10.1371/journal.pone.0027308.
68. Ho AL, Adkins D, Lorch JH, Thomas JS, Grewal JS. A phase 2 open-label study of conditionally active biologic ozuriftamab vedotin (BA3021) in failed PD-1/L1 treatment of patients with recurrent or metastatic squamous cell carcinoma of the head and neck. Journal of Clinical Oncology **2023**;41(16_suppl):TPS6107-TPS doi 10.1200/JCO.2023.41.16_suppl.TPS6107.
69. Goydel RS, Weber J, Peng H, Qi J, Soden J, Freeth J*, et al.* Affinity maturation, humanization, and co-crystallization of a rabbit anti-human ROR2 monoclonal antibody for therapeutic applications. J Biol Chem **2020**;295(18):5995-6006 doi 10.1074/jbc.RA120.012791.
70. Wei W, Li H, Li N, Sun H, Li Q, Shen X. WNT5A/JNK signaling regulates pancreatic cancer cells migration by Phosphorylating Paxillin. Pancreatology **2013**;13(4):384-92 doi 10.1016/j.pan.2013.05.008.
71. Franses JW, Philipp J, Missios P, Bhan I, Liu A, Yashaswini C*, et al.* Pancreatic circulating tumor cell profiling identifies LIN28B as a metastasis driver and drug target. Nat Commun **2020**;11(1):3303 doi 10.1038/s41467-020-17150-3.
72. Huang L, Bockorny B, Paul I, Akshinthala D, Frappart PO, Gandarilla O*, et al.* PDX-derived organoids model in vivo drug response and secrete biomarkers. JCI Insight **2020**;5(21) doi 10.1172/jci.insight.135544.
73. Huang L, Holtzinger A, Jagan I, BeGora M, Lohse I, Ngai N*, et al.* Ductal pancreatic cancer modeling and drug screening using human pluripotent stem cell- and patient-derived tumor organoids. Nat Med **2015**;21(11):1364-71 doi 10.1038/nm.3973.
74. Slaymaker IM, Gao L, Zetsche B, Scott DA, Yan WX, Zhang F. Rationally engineered Cas9 nucleases with improved specificity. Science **2016**;351(6268):84-8 doi 10.1126/science.aad5227.
75. Ho HY, Susman MW, Bikoff JB, Ryu YK, Jonas AM, Hu L*, et al.* Wnt5a-Ror-Dishevelled signaling constitutes a core developmental pathway that controls tissue morphogenesis. Proc Natl Acad Sci U S A **2012**;109(11):4044-51 doi 10.1073/pnas.1200421109.
76. Steele NG, Biffi G, Kemp SB, Zhang Y, Drouillard D, Syu L*, et al.* Inhibition of Hedgehog Signaling Alters Fibroblast Composition in Pancreatic Cancer. Clin Cancer Res **2021**;27(7):2023-37 doi 10.1158/1078-0432.CCR-20-3715.
77. Germain PL, Lun A, Garcia Meixide C, Macnair W, Robinson MD. Doublet identification in single-cell sequencing data using scDblFinder. F1000Res **2021**;10:979 doi 10.12688/f1000research.73600.2.

Downloaded from http://aacrjournals.org/cancerdiscovery/article-pdf/doi/10.1158/2159-8290.CD-24-0137/3472265/cd-24-0137.pdf by Cold Spring Harbor Laboratory user on 15 July 2024

78. Thibodeau A, Eroglu A, McGinnis CS, Lawlor N, Nehar-Belaid D, Kursawe R*, et al.* AMULET: a novel read count-based method for effective multiplet detection from single nucleus ATAC-seq data. Genome Biol **2021**;22(1):252 doi 10.1186/s13059-021-02469-x.
79. Hao Y, Hao S, Andersen-Nissen E, Mauck WM, 3rd, Zheng S, Butler A*, et al.* Integrated analysis of multimodal single-cell data. Cell **2021**;184(13):3573-87 e29 doi 10.1016/j.cell.2021.04.048.
80. Waltman L, van Eck NJ. A smart local moving algorithm for large-scale modularity-based community detection. The European Physical Journal B **2013**;86(11):471 doi 10.1140/epjb/e2013-40829-0.
81. Zhang Y, Parmigiani G, Johnson WE. ComBat-seq: batch effect adjustment for RNA-seq count data. NAR Genom Bioinform **2020**;2(3):lqaa078 doi 10.1093/nargab/lqaa078.
82. Pfaffl MW. A new mathematical model for relative quantification in real-time RT-PCR. Nucleic Acids Res **2001**;29(9):e45 doi 10.1093/nar/29.9.e45.
83. Ewels P, Magnusson M, Lundin S, Kaller M. MultiQC: summarize analysis results for multiple tools and samples in a single report. Bioinformatics **2016**;32(19):3047-8 doi 10.1093/bioinformatics/btw354.
84. Patro R, Duggal G, Love MI, Irizarry RA, Kingsford C. Salmon provides fast and bias-aware quantification of transcript expression. Nat Methods **2017**;14(4):417-9 doi 10.1038/nmeth.4197.
85. Love MI, Huber W, Anders S. Moderated estimation of fold change and dispersion for RNA-seq data with DESeq2. Genome Biol **2014**;15(12):550 doi 10.1186/s13059-014-0550-8.
86. SOM PAK: The Self-Organizing Map Program Package. [cited 2024 May 05]. Available from: https://ntrl.ntis.gov/NTRL/dashboard/searchResults/titleDetail/PB96173927.xhtml
87. Langmead B, Salzberg SL. Fast gapped-read alignment with Bowtie 2. Nat Methods **2012**;9(4):357-9 doi 10.1038/nmeth.1923.
88. Dobin A, Davis CA, Schlesinger F, Drenkow J, Zaleski C, Jha S*, et al.* STAR: ultrafast universal RNA-seq aligner. Bioinformatics **2013**;29(1):15-21 doi 10.1093/bioinformatics/bts635.
89. Anders S, Pyl PT, Huber W. HTSeq--a Python framework to work with high-throughput sequencing data. Bioinformatics **2015**;31(2):166-9 doi 10.1093/bioinformatics/btu638.
90. Wolf FA, Angerer P, Theis FJ. SCANPY: large-scale single-cell gene expression data analysis. Genome Biol **2018**;19(1):15 doi 10.1186/s13059-017-1382-0.
91. Korsunsky I, Millard N, Fan J, Slowikowski K, Zhang F, Wei K*, et al.* Fast, sensitive and accurate integration of single-cell data with Harmony. Nat Methods **2019**;16(12):1289-96 doi 10.1038/s41592-019-0619-0.
92. Gu Z, Gu L, Eils R, Schlesner M, Brors B. circlize Implements and enhances circular visualization in R. Bioinformatics **2014**;30(19):2811-2 doi 10.1093/bioinformatics/btu393.
93. Subramanian A, Tamayo P, Mootha VK, Mukherjee S, Ebert BL, Gillette MA*, et al.* Gene set enrichment analysis: a knowledge-based approach for interpreting

Downloaded from http://aacrjournals.org/cancerdiscovery/article-pdf/doi/10.1158/2159-8290.CD-24-0137/3472265/cd-24-0137.pdf by Cold Spring Harbor Laboratory user on 15 July 2024

genome-wide expression profiles. Proc Natl Acad Sci U S A **2005**;102(43):15545-50 doi 10.1073/pnas.0506580102.
94. Sherman BT, Hao M, Qiu J, Jiao X, Baseler MW, Lane HC*, et al.* DAVID: a web server for functional enrichment analysis and functional annotation of gene lists (2021 update). Nucleic Acids Res **2022**;50(W1):W216-W21 doi 10.1093/nar/gkac194.
95. Huang da W, Sherman BT, Lempicki RA. Systematic and integrative analysis of large gene lists using DAVID bioinformatics resources. Nat Protoc **2009**;4(1):44-57 doi 10.1038/nprot.2008.211.

Figure Legends

Figure 1

Tracking cell identity changes in early pancreatic cancer development by using snATAC-seq. **A,** Representative H&E staining of indicated mouse genotypes. Eight- to 9-week-old animals were given Tamoxifen to induce *Cre*^{ERT}-mediated recombination and were sacrificed 2 and 10 weeks later. Scale bars, 50 µm. **B,** Representative multiplex IHC staining for Amylase (yellow), Krt19 (teal) and Vimentin (brown). Scale bars, 50 µm. **C,** Unsupervised clustering of snATAC-seq data from indicated mouse genotypes (n=2 each), represented as UMAP plots. Indicated cell types were identified. **D,** Dot plot showing average gene expression and percentage of cells expressing selected marker genes across all identified clusters. **E,** Percentage distribution of nuclei in each annotated cell cluster was determined over the total amount of nuclei in each genotype and time point (n=2).

Figure 2

Ablation of *Pdx1* initiates gastric transdifferentiation. **A,** UMAP analysis depicting acinar cell clusters from indicated mouse genotypes, 2 weeks post Tamoxifen. **B,** Heatmaps showing expression levels of genes, that showed highest correlation in both snATAC-seq (upper panel) and bulk RNA-seq datasets (lower panel). Expression levels are represented by color coding. **C,** Heatmap depicting mRNA expression of selected acinar and gastric lineage genes. **D,** UMAP plots using scRNA-seq data from mouse stomach cells (19) with gastric cell type signature annotation (34). **E,** Gene set enrichment

Downloaded from http://aacrjournals.org/cancerdiscovery/article-pdf/doi/10.1158/2159-8290.CD-24-0137/3472265/cd-24-0137.pdf by Cold Spring Harbor Laboratory user on 15 July 2024

analysis results for SPEM signature comparing *Ptf1a^{ERT};K** and *Ptf1a^{ERT};K*;Pdx1$^{f/f}$* acinar cells.

Figure 3

Ror2 marks gastric neck cell and SPEM signatures in pancreatic neoplasia. **A,** Representative images of *Ror2* RNA-ISH in combination with Krt19 IHC (upper panel) and Ror2 IHC (lower panel) of pancreatic tissue from *Ptf1a^{ERT};K** mice harvested at indicated time points post Tamoxifen. Scale bars, 50 µm. Percentage of Krt19-positive cells with ≥ 5 puncta was quantitated. **B,** UMAP analysis depicting epithelial cell clusters of *Ptf1a^{ERT};K** mice from Schlesinger et al. scRNA-seq dataset (19) (left panel). TdTomato-positive meta/neoplastic cells were subsetted and *Ror2* expression and enrichment of gastric neck (34) and SPEM cell signature is shown. **C,** UMAP analysis illustrating subcluster identities of tdTomato-positive meta/neoplastic cells from Schlesinger et al. scRNA-seq dataset (19) after integration with Harmony. **D,** Heatmap representing expression of *Ror2* and of top 10 most significantly *Ror2*-correlating genes across identified Harmony clusters. **E,** UMAP analysis showing expression of *Muc6* in tdTomato-positive meta/neoplastic cells from Schlesinger et al. scRNA-seq dataset (19). **F,** Multiplex IF and RNA-ISH staining for Krt19 (green), *Muc6* (white) and *Ror2* (red) on tissue of a *Ptf1a^{ERT};K** mouse, 20 weeks post Tamoxifen. **G,** Image showing Ki67 (purple) and Ror2 (brown) IHC. **H,** Dual IHC depicting Tff1 (teal) and Ror2 (brown) staining. **I,** Cdkn2a (green) and Ror2 (brown) dual IHC staining. For all dual IHC staining, the percentage of single- and dual-positive cells in ductal cells were quantified. For all staining, representative images are depicted. Scale bars, 50 µm. All data are presented as mean ± SEM; p-values were calculated by two-tailed, unpaired Student's t-test; * $p < 0.05$.

Figure 4

Ror2 ablation shifts gastric metaplasia towards a pit cell identity. **A,** H&E staining of *Ptf1a^{ERT};K** and *Ptf1a^{ERT};K*;Ror2$^{f/f}$* mice, 20 and 40 weeks after Tamoxifen administration. Tissue remodeling and number of mucinous and non-mucinous lesions were quantified (n=5-11). **B,** Dual IHC staining for Ki67 (brown) and Krt19 (teal). **C,**

Downloaded from http://aacrjournals.org/cancerdiscovery/article-pdf/doi/10.1158/2159-8290.CD-24-0137/3472265/cd-24-0137.pdf by Cold Spring Harbor Laboratory user on 15 July 2024

Images depicting dual Cdkn2a (brown) and Krt19 (teal) IHC staining. **D,** Multiplex RNA-ISH and IHC staining detecting *Muc6* mRNA expression (red) and Krt19 (teal) in mice, sacrificed 40 weeks post Tamoxifen. **E,** Dual IHC staining for Muc5ac (brown) and Krt19 (green). **F,** Images showing Tff1 (brown) and Krt19 (teal) dual IHC. **G,** Immunoblot analysis for Tff1 and Krt19 from protein lysates of *Ptf1a^{ERT};K** and *Ptf1a^{ERT};K*;Ror2$^{f/f}$* mice, sacrificed 40 weeks post Tamoxifen (n=4). Vinculin served as loading control. For all staining, representative images are depicted. Scale bars, 50 µm. Staining were quantified with HALO software and all data are presented as mean ± SEM; p-values were calculated by two-tailed, unpaired Student's *t*-test; * $p < 0.05$, ** $p < 0.01$, *** $p < 0.001$.

Figure 5

Pit cell identity marks the classical subtype of PDAC whereas *Ror2* expression is associated with the basal-like subtype. **A,** Representative images of dual IHC staining for Tff1 (teal) and Ror2 (brown) on tissue of *KPC* mice. Scale bars, 50 µm. **B,** Pearson correlation scatter plots showing correlation of *Ror2* to *Tff1* gene expression in pancreatic cancer cell lines. RNA-seq data from Mueller et al. (42), correlation coefficient and p-value are indicated. **C,** Heatmap depicting expression of top 50 most enriched genes in meta/neoplastic pit-like cells from Schlesinger et al. scRNA-seq dataset (19) in pancreatic cancer cell lines (42). PDAC subtype annotation was performed with gene signatures from Moffitt et al. (23). **D,** UMAP plots indicating expression signatures of meta/neoplastic pit-like cells (19) and indicated PDAC subtypes retrieved from Ragharan et al. (27) in 174 human scRNA-seq PDAC samples (2,43-51). **E,** Heatmap using RNA-seq data from Mueller et al. (42), showing expression of top 50 genes that most significantly positively or negatively correlate with *Ror2*. For subtype annotation, gene signatures from Moffitt et al. (23) were used. **F,** Correlation of *Ror2* expression to indicated genes was determined by Pearson correlation. RNA-seq data from Mueller et al. (42) was used.

Figure 6

Downloaded from http://aacrjournals.org/cancerdiscovery/article-pdf/doi/10.1158/2159-8290.CD-24-0137/3472265/cd-24-0137.pdf by Cold Spring Harbor Laboratory user on 15 July 2024

ROR2 induces EMT and stemness in human pancreatic cancer cells. **A,** Representative brightfield images of ROR2 IHC staining. Scale bars, 50 µm. **B,** Correlation plots showing correlation of *ROR2* mRNA expression to indicated genes in micro-dissected, epithelial PDAC compartment using RNA-sequencing data from Maurer et al. (52). **C,** mRNA expression of *ROR2*, *ZEB1*, *VIM*, and *CDH1* was determined in indicated human PDAC and organoid lines by performing qRT-PCR. Expression values were calculated in relation to the housekeeper gene *GAPDH* (n=3). **D,** Representative immunoblot analysis of indicated proteins using protein lysates of HPAF-II, UM32, PANC1 and UM5 cells. GAPDH served as loading control. **E,** Brightfield images of control and ROR2-overexpressing HPAF-II and UM32 cells (upper panel). Scale bars, 200 µm. Immunofluorescence staining for CDH1 (green), VIM (red) and nuclei (Hoechst 33342, blue) of indicated cell lines (lower panel). Scale bars, 37.6 µm. **F,** Representative immunoblot analysis detecting ROR2, VIM, ZEB1 and CDH1 protein levels in control and ROR2-overexpressing HPAF-II and UM32 cells. GAPDH served as loading control. **G,** Transcriptomic signatures of control and ROR2-overexpressing HPAF-II and UM32 cells were compared to EMT score, established by Groger et al. (53). p-values were calculated by Mann-Whitney test. **H,** Sphere-forming efficiency of control and ROR2-overexpressing HPAF-II and UM32 cells is depicted as number of spheres in relation to total number of seeded wells (n=3). Diameter for every sphere was determined. Data are presented as mean ± SEM; p-values were calculated by two-tailed, unpaired Student's *t*-test; * $p < 0.05$, **** $p < 0.0001$.

Figure 7

ROR2 confers a RAS-independent, AKT-dependent proliferative phenotype. **A,** Cell confluency of PANC1 and UM5 control and ROR2 knockout cells using two different guide RNAs (ROR2 KO #1, ROR2 KO #2) was measured every 2 hours over a period of 6 days (n=4). Each data point was calculated as relative cell confluency in relation to the first measurement. Statistical significance was determined for the last measurement. **B,** Cell confluency of control and ROR2-overexpressing HPAF-II and UM32 cells was monitored for a total of 6 days. Statistical significance was determined for the last measurement. **C,** Representative immunoblot analysis for ROR2 and indicated signaling

Downloaded from http://aacrjournals.org/cancerdiscovery/article-pdf/doi/10.1158/2159-8290.CD-24-0137/3472265/cd-24-0137.pdf by Cold Spring Harbor Laboratory user on 15 July 2024

proteins in PANC1 and UM5 control and ROR2 knockout cells. GAPDH served as loading control. **D,** Representative immunoblot analysis showing expression levels and phosphorylation status of indicated signaling pathway regulators in control and ROR2-overexpressing HPAF-II and UM32 cells. GAPDH served as loading control. **E,** Control and ROR2-overexpressing HPAF-II and UM32 cells were treated with increasing concentrations of $KRAS^{G12D}$ inhibitor MRTX1133 and dose-response curves were established (n=3). For each experiment, area under curve (AUC) was determined. **F,** Dose-response curves after treating control and ROR2-overexpressing HPAF-II and UM32 cells with indicated concentrations of AKT inhibitor MK-2206 (n=3). For each experiment, AUC was determined. Unless stated otherwise, all data are presented as mean ± SEM; p-values were calculated by two-tailed, unpaired Student's *t*-test; * $p < 0.05$, ** $p < 0.01$, *** $p < 0.001$, **** $p < 0.0001$.

Downloaded from http://aacrjournals.org/cancerdiscovery/article-pdf/doi/10.1158/2159-8290.CD-24-0137/3472265/cd-24-0137.pdf by Cold Spring Harbor Laboratory user on 15 July 2024

Figure 1

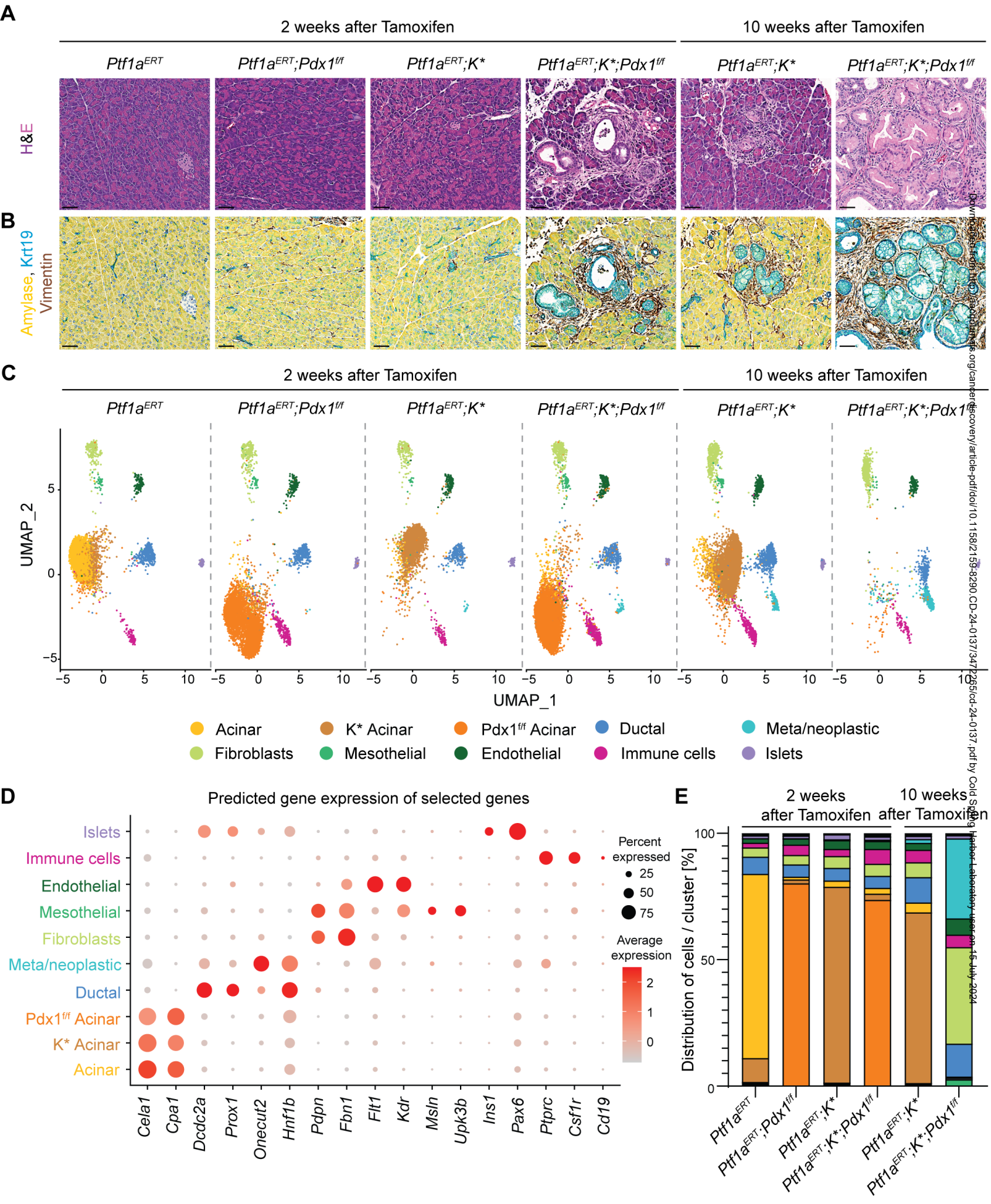

Downloaded from http://aacrjournals.org/cancerdiscovery/article-pdf/doi/10.1158/2159-8290.CD-24-0137/3472265/cd-24-0137.pdf by Cold Spring Harbor Laboratory user on 15 July 2024

Figure 2

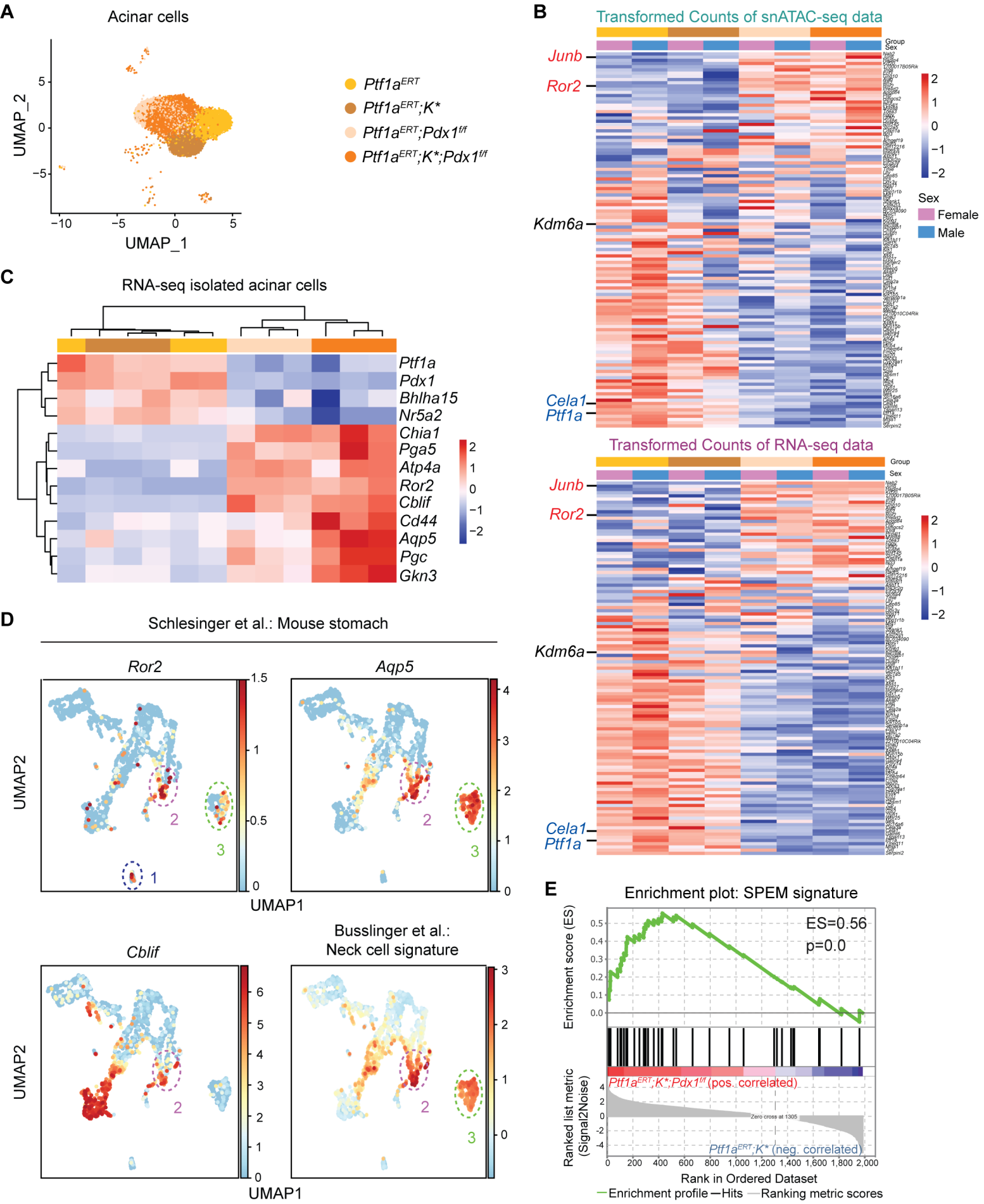

Downloaded from http://aacrjournals.org/cancerdiscovery/article-pdf/doi/10.1158/2159-8290.CD-24-0137/3472265/cd-24-0137.pdf by Cold Spring Harbor Laboratory user on 15 July 2024

Figure 3

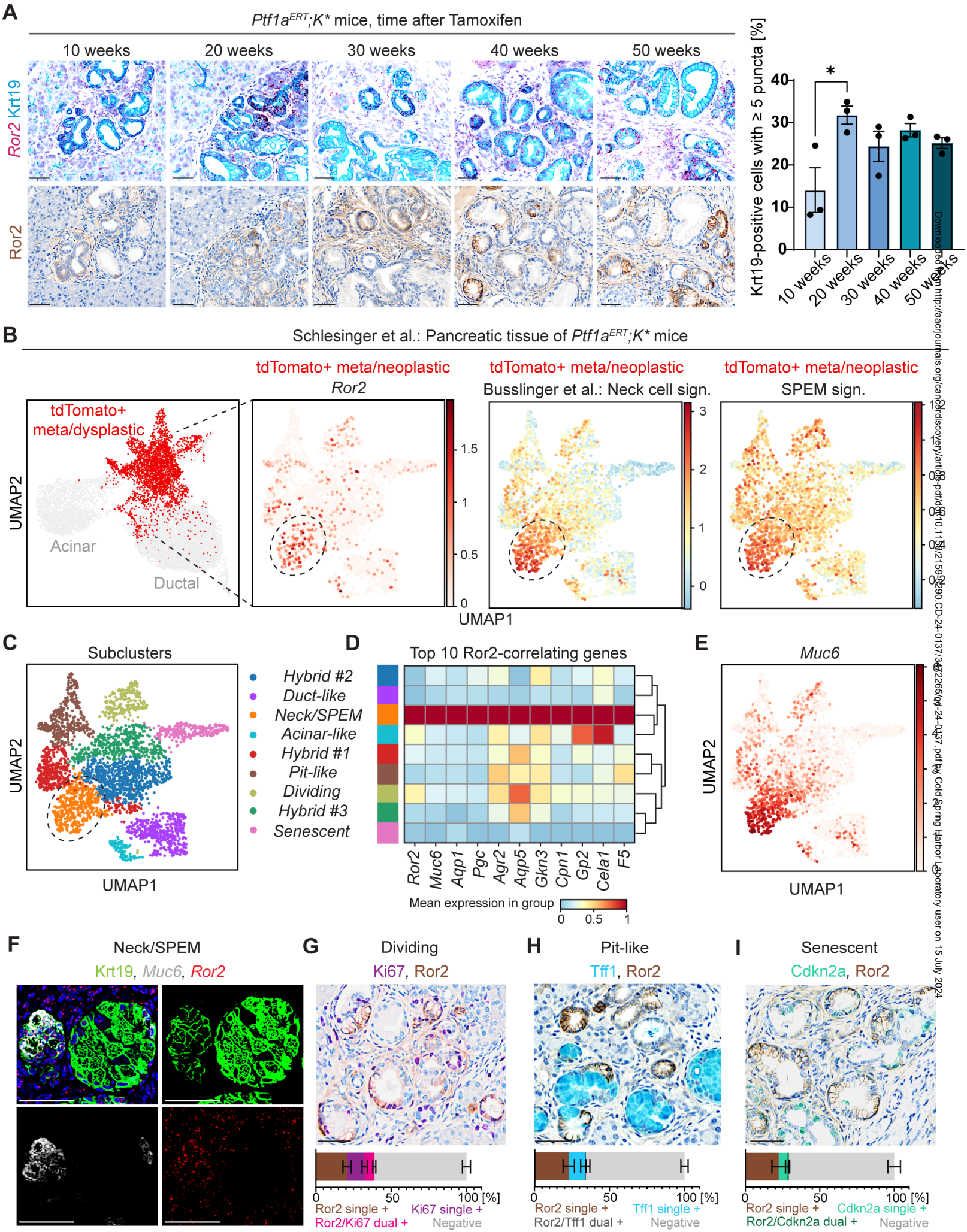

Downloaded from http://aacrjournals.org/cancerdiscovery/article-pdf/doi/10.1158/2159-8290.CD-24-0137/3422655/cd-24-0437.pdf by Cold Spring Harbor Laboratory user on 15 July 2024

Figure 4

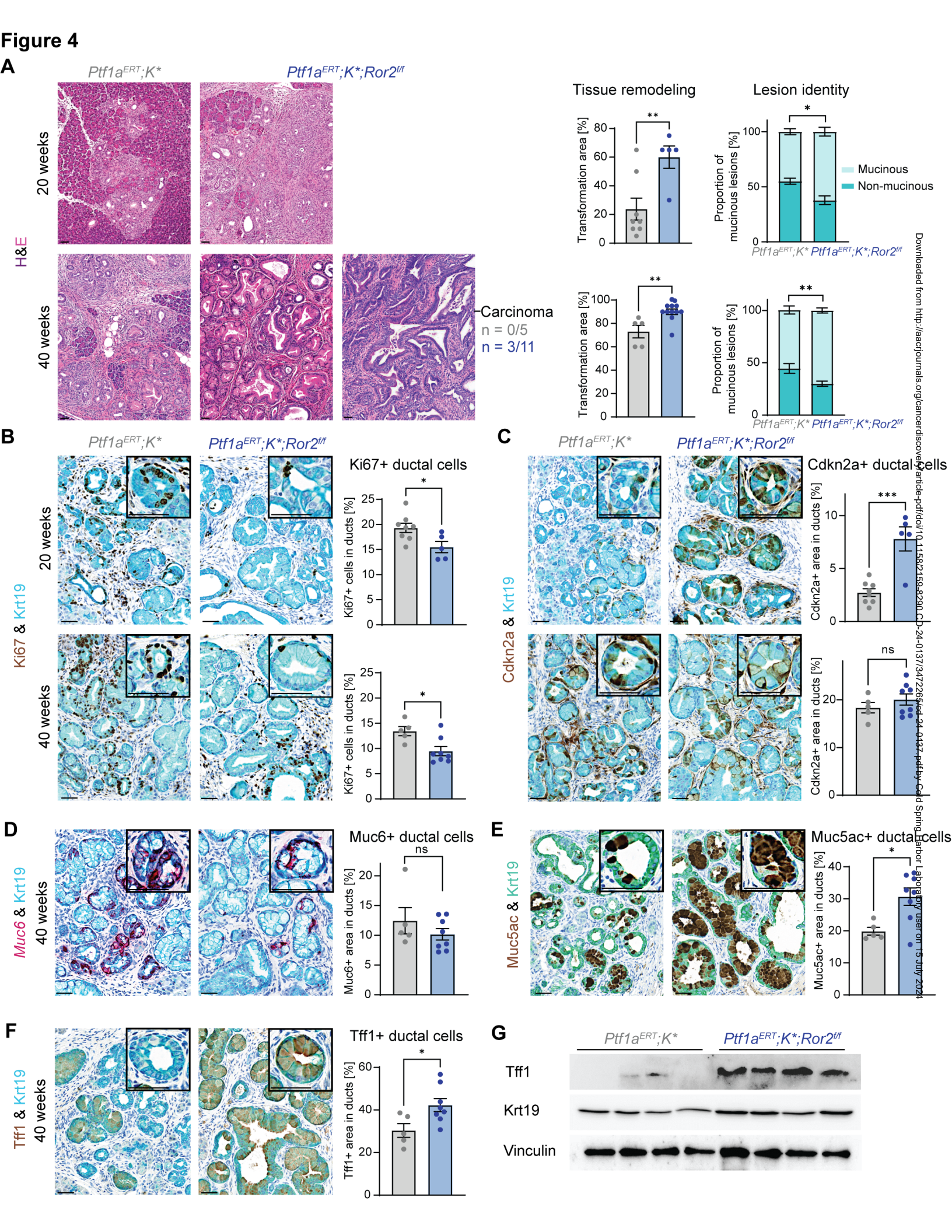

Downloaded from http://aacrjournals.org/cancerdiscovery/article-pdf/doi/10.1158/2159-8290.CD-24-0137/3472265/cd-24-0137.pdf by Cold Spring Harbor Laboratory user on 15 July 2024

Figure 5

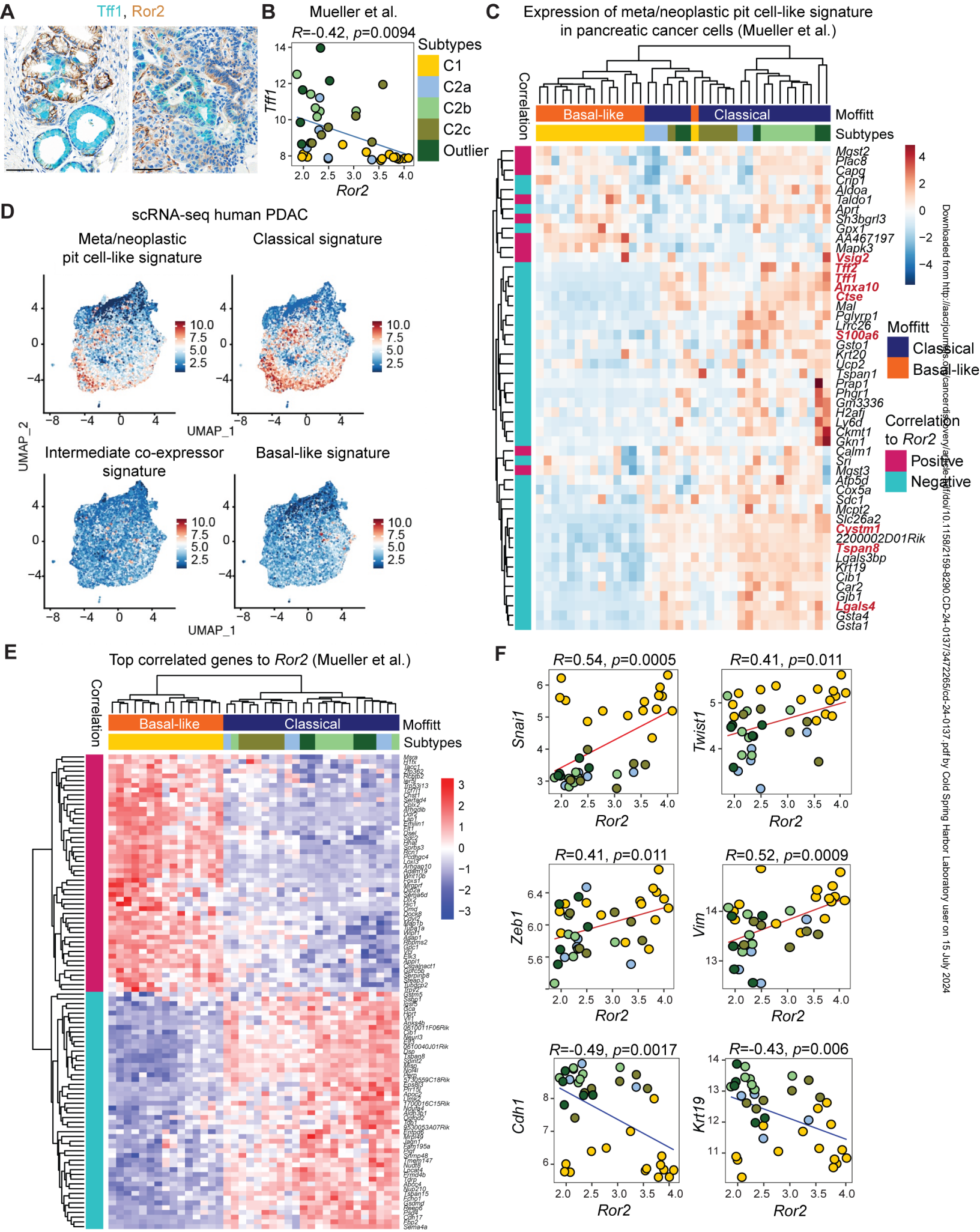

Downloaded from http://aacrjournals.org/cancerdiscovery/article-pdf/doi/10.1158/2159-8290.CD-24-0137/3472265/cd-24-0137.pdf by Cold Spring Harbor Laboratory user on 15 July 2024

Figure 6

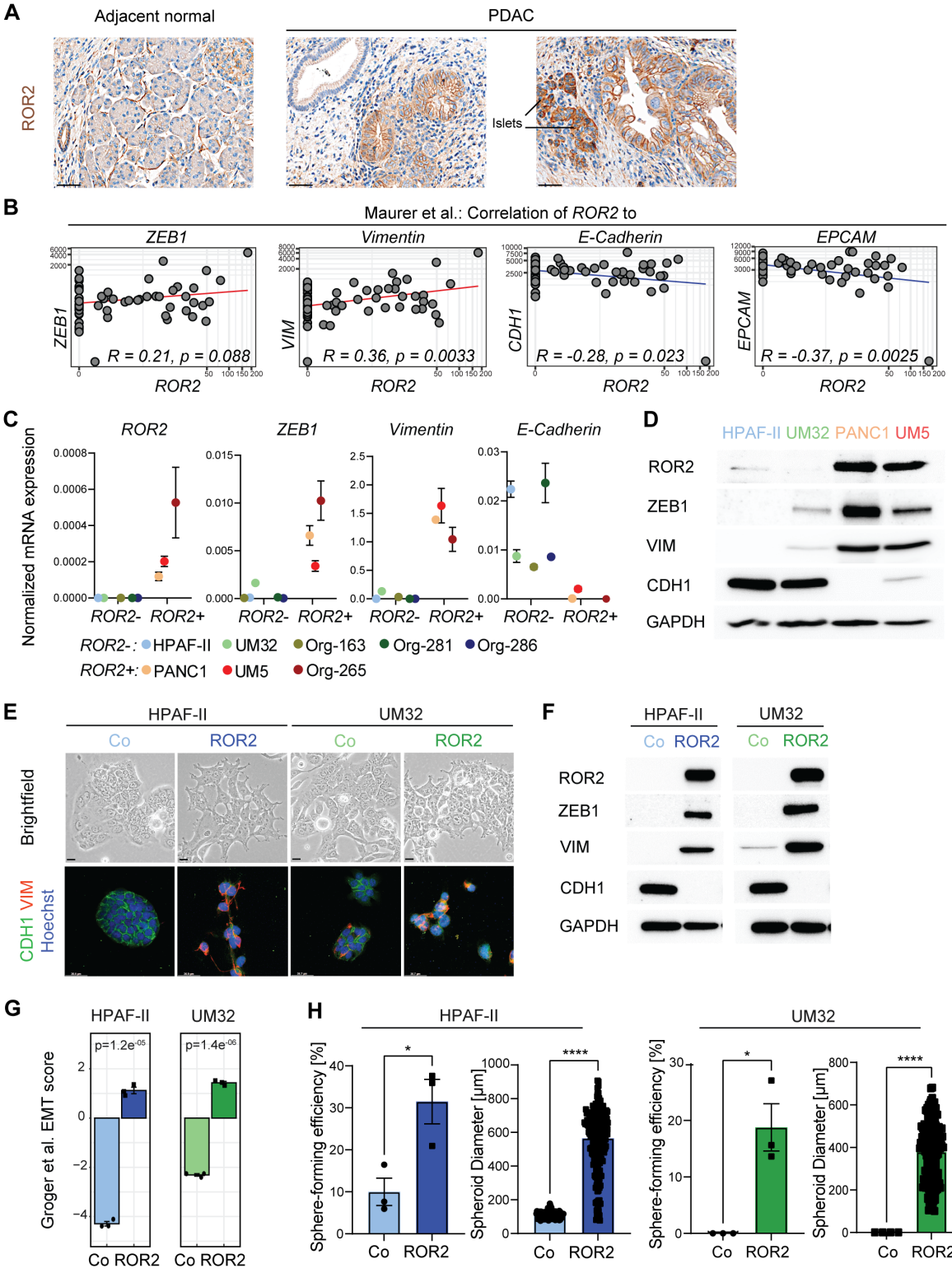

Downloaded from http://aacrjournals.org/cancerdiscovery/article-pdf/doi/10.1158/2159-8290.CD-24-0137/3472265/cd-24-0137.pdf by Cold Spring Harbor Laboratory user on 15 July 2024

Figure 7

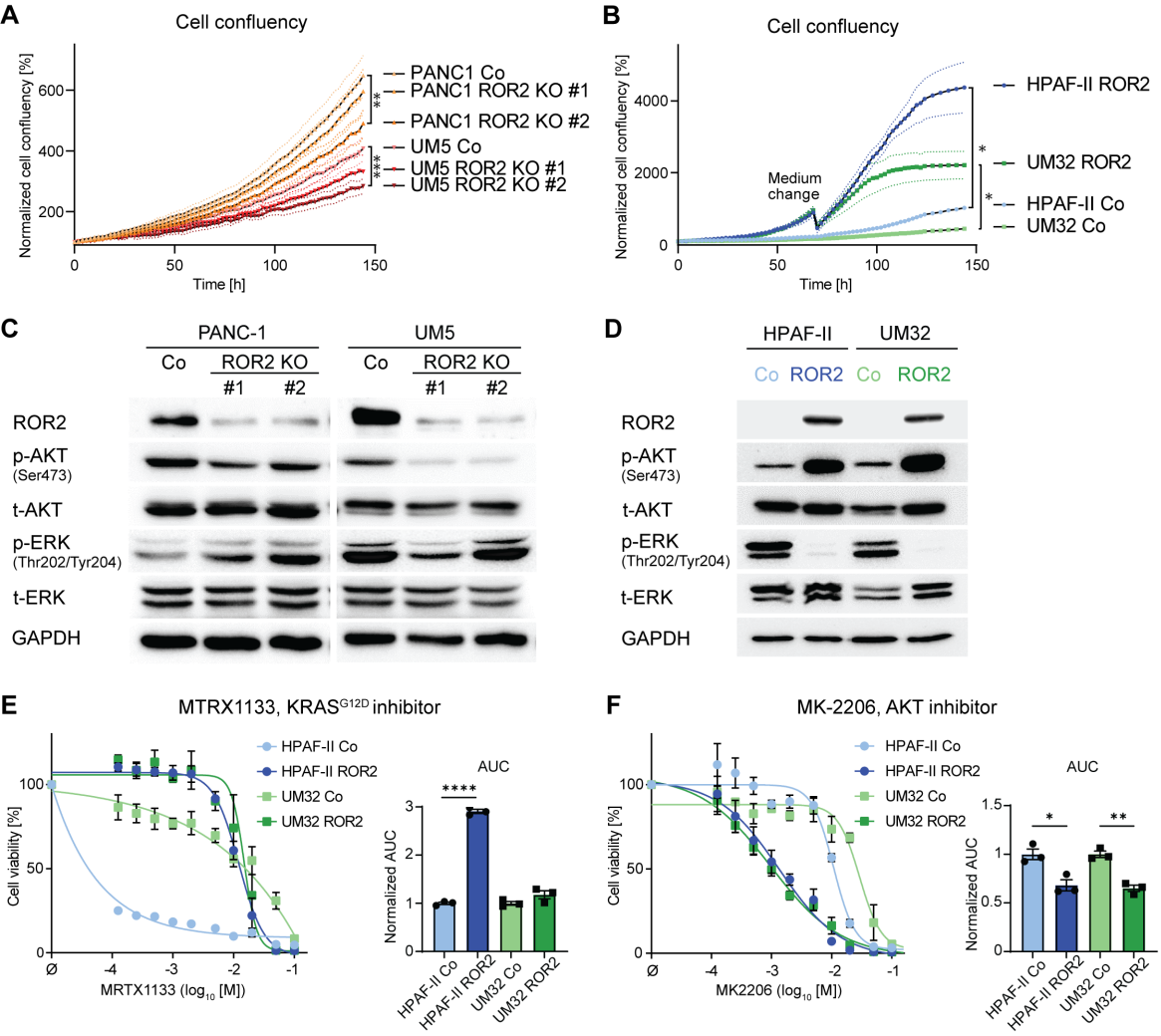

Downloaded from http://aacrjournals.org/cancerdiscovery/article-pdf/doi/10.1158/2159-8290.CD-24-0137/3472265/cd-24-0137.pdf by Cold Spring Harbor Laboratory user on 15 July 2024